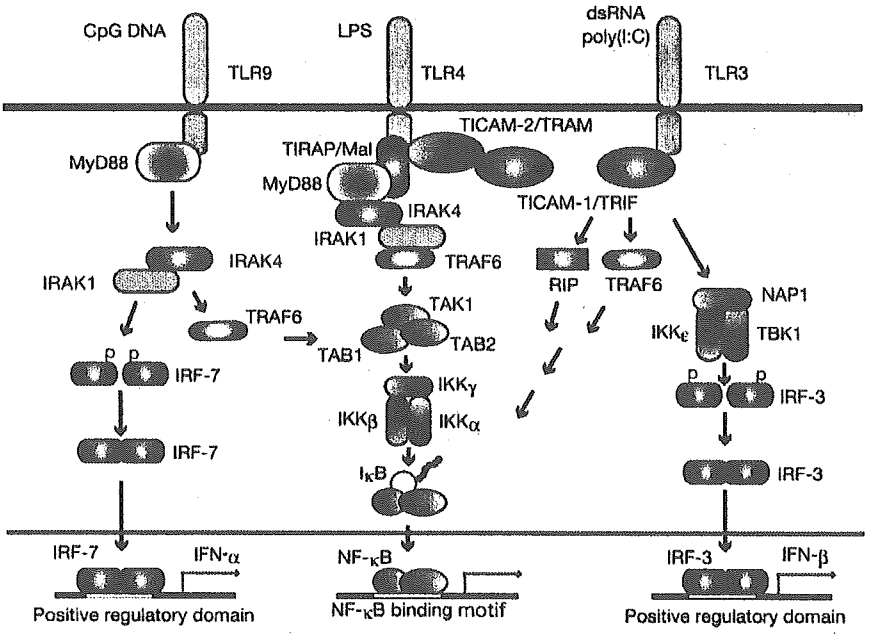

Fig. 1. **Possible signaling pathways coupling TLRs to IFN induction.** TLR9 (also possibly TLR7) can signal exclusively via MyD88 to activate IRF-7 and NF-κB. IRF-7 activation activates the IFN-α promoter in pDCs. TLR3 uses TICAM-1 but not MyD88 in mDCs to induce activation of IRF-3 and the IFN-β promoter. TICAM-1 can recruit RIP1, which together with TRAF6 activates NF-κB. TLR4 can signal via both MyD88 and TICAM-1 in mDCs. Mal/TIRAP and TICAM-2 are adapters involved in coupling TLR4 to MyD88 and TICAM-1, respectively. Either MyD88 or TICAM-1 promotes activation of NF-κB and MAPKs, leading to transcription of cytokine genes. TICAM-1 in the TLR4 pathway also activates IRF-3, allowing weak IFN-β production.

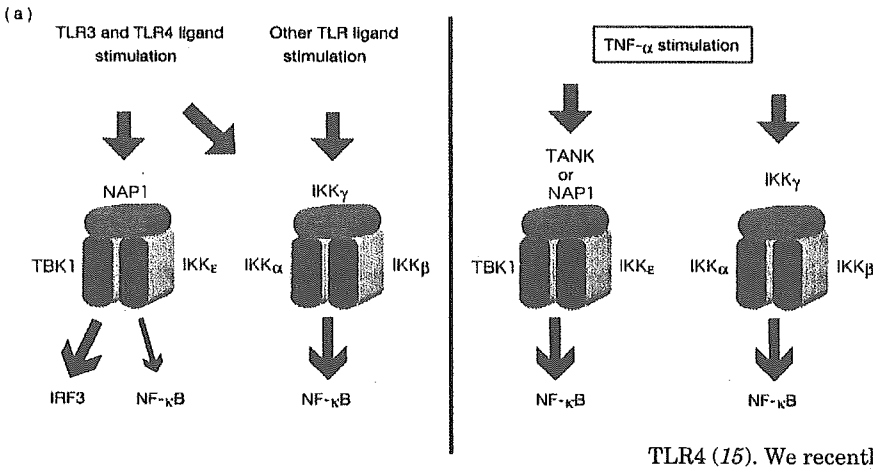

(b)

% identity	TANK	IKKγ
NAP1	18.2	20.3
TANK	—	17.1

Fig. 2. **Trimolecular interactions of two kinases and their regulatory subunits in the TLR pathway.** IKKγ, TANK and NAP1 do not act as kinases, but act as regulatory subunits for kinase complexes. TBK1 and IKKε (or IKKi) assemble with NAP1 or TANK to activate IRF-3 and to a lesser extent NF-κB. IRF-3 is preferentially activated in the TLR pathway. IKKγ couples with IKKα and IKKβ, which allows the activation of NF-κB. IRF-3/7 are not activated via this complex. The three non-kinase subunits are structurally similar to one another.

also IRF-3 (*12*, *13*). Judging from their similarity and analogy, we here hypothesize that the two kinase complexes similarly assemble, at least in a certain situation. On infection, viruses activate type I IFN, possibly *via* so-called virus-activated kinase (VAK) involving IKKε and TBK1, and IRF-3 and IRF-7 (*14*). We will focus on how the TLR3-TICAM-1 pathway links the kinases that activate IRF-3 during viral infection, and then summarize the structure-function relations of the family of molecules that bridge TICAM-1 and IRF-3-activating kinases.

Downstream of TICAM-1—TICAM-1 is an essential molecule for IFN-β production through TLR3 and TLR4 (*15*). We recently reported that NAP1 interacts with TICAM-1 (*16*). It has been reported that NAP1 directly interacts with TBK1 (also called NAK) and triggers NF-κB activation through TBK1 (*17*). TICAM-1 recruits NAP1, either directly or indirectly, to its N-terminal region. NAP1 forms a trimolecular complex with IKKε and TBK1, and this complex mainly targets IRF-3. Besides IRF-3 activation, TICAM-1 induces NF-κB and MAPK activation. There are three molecules that reportedly participate in NF-κB activation through TICAM-1. Firstly, the NAP1 complex binds TICAM-1 to activate NF-κB in the TLR3 pathway (*16*) in a manner similar to in the TNF-α-inducing pathway that involves the TBK1/IKKε complex (*17*). Secondly, TRAF6 interacts with the N-terminal region of TICAM-1 and then mediates NF-κB activation (*18*). TRAF6 binds IRAK1/4, activates the TAK/TAB1/TAB2 complex, and subsequently activates the IKKα/β/γ complex on TLR4-ligand stimulation. This trimolecular complex degrades IκB and liberates NF-κB. It is notable that IRAK1 and IRAK4 are not involved in

TLR3-mediated signaling. After ubiquitination, TRAF6 may interact with other molecules besides IRAK1/4 and form a complex with IKKα/β/γ (*19*). Thirdly, RIP1 binds TICAM-1 *via* a RIP homotypic interaction motif (PHIM) domain located in its C-terminal region (*20*). RIP1 associates with TRADD, leading to activation of the IKKα/β/γ complex following TNF-α stimulation, and leading finally to NF-κB activation. Thus, two different kinase complex properties effectively function downstream of TICAM-1 in the NF-κB activation pathway. The reported kinase complex consisting of TANK, IKKε and TBK1 should therefore be present in addition to the complex of NAP1, IKKε and TBK1. However, the role and function of the former complex downstream of TICAM-1 remain to be elucidated.

The Properties of the Kinase Complex—The three molecules NAP1, TANK and IKKγ show significant structural similarities, suggesting that they comprise a protein family with similar functional characteristics (Fig. 2a). In most cell types, for activation of TBK1 and IKKε leading to IRF-3-mediated IFN-β induction, NAP1 plays the main role in TBK1/IKKε-driven signaling. Similar to NAP1, TANK has been reported to assemble with TBK1 and IKKε (*21*, *22*). However, TANK does not form a molecular complex with TICAM-1 in HEK293 or other cells (*16*). Thus, the functional properties of the TANK-TBK1-IKKε complex, if any, have not been well characterized. It is likely that this complex is placed downstream of other adapter or DNA/RNA-binding proteins.

Structurally, NAP1 is 20.3% similar to IKKγ and 18.2% similar to TANK (Fig. 2b). NAP1 consists of 391 a.a. (*17*), TANK of 426 a.a. (*21*), and IKKγ of 419 a.a. (*23*). Their TBK1-binding regions have been reported to reside within 158-270 in NAP1 and 1-190 in TANK. The IKKα/β-binding region is within 44-85 in IKKγ (Fig. 3). Comparison of the a.a. sequences of these three proteins suggested that

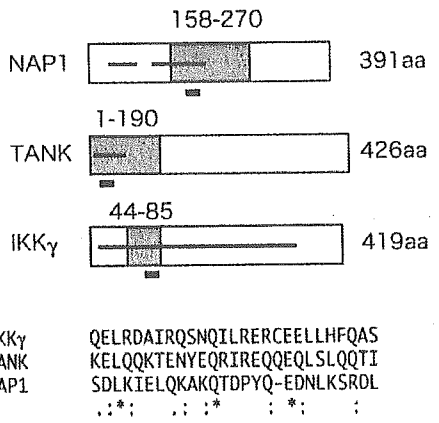

Fig. 3. **Seqence similarity between the three regulatory subunits.** NAP1 consists of 391 a.a. and binds TBK1 in the region of 158-270 a.a. (17). TANK is a 426 a.a. protein with binding capacity as to TBK1 at 1-190 a.a. (21). IKK-γ comprises 419 a.a., and its IKKβ-binding region has been identified as 44-85 a.a. (23). Clustal W alignment analysis suggested the presence of a highly conserved region in these family proteins. This conserved region lies within the predicted coiled-coil region in each protein. Solid bars, coiled coil regions; gray boxes, reported TBK1- or IKKβ-binding regions; thick underlines, the highly conserved regions in the TBK1 and IKKγ-binding sites, the sequences of which are shown below the picture.

there are sequence-conserved regions in the TBK-binding regions of these proteins (Fig. 3). The conserved regions are located within the expected coiled-coil domain, supporting the previous notion that these three molecules bind kinase molecules to regulate downstream signaling (*17*, *21*, *23*). The mechanism underlying differential selection of kinase complexes by each regulatory protein, however, remains undetermined.

IFN-β Induction via Virus Infection—Virus infection generally causes IFN-α/β production. This has been confirmed using various species of RNA viruses and some DNA viruses. The TLR3-TICAM-1 pathway is crucial in mCMV infection (*24*). This pathway may participate in Westnile virus and influenzavirus infections (*25*, *26*). Interestingly, TICAM-1 is a substrate of NS3/4A protease of HCV (*27*). Poly(I:C) as well as dsRNA appear to activate IRF-3 at least in part via the TLR3-TICAM-1 pathway. Such activation occurs even when they are exogenously added. However, poly(I:C) introduced into the cytoplasm of mDC induces strong activation of IRF-3 and type-I IFN induction even without TLR3 (*28*). Thus, the TLR3-independent pathway for activation of IRF-3 should be present inside the cells.

Recently, a CARD domain-containing helicase named RIG-I was reported to participate in signaling for TLR3-independent IFN-β-induction. RIG-I recognizes dsRNA in the helicase domain and induces activation of IRF-3 in the CARD domain (*29*). Similar results are obtained with another RIG-I family protein, MDA5, in Sendai and some other virus species (*30*). PKR might participate in dsRNA-mediated IFN-α/β induction (*31*). Thus, it remains unclear if RIG-I represents the TLR3-independent IRF-3 activation pathway. In the TLR3-TICAM-1 pathway, NAP1 downstream of TICAM-1 participates in poly(I:C)-dependent intracellular activation of IRF-3. The RIG-I pathway was examined using several viruses and polyI:C, and the NAP1-IKKε/TBK1-IRF-3 pathway was found to participate in TLR3-independent IFN-β induction (*32*). In the model proposed by Nakanishi *et al.* (*33*), NAP1 assembles with TBK1 and IKKε kinases to activate NF-κB. This and a recent report (*32*) suggest that the NAP1-TBK1-IKKε complex is placed downstream of both TICAM-1 and RIG-I/MDA5, resulting in IFN-β production. This kinase complex, called virus-activated kinase (VAK), acts *via* both intra- and extra-cellular routes to activate IRF-3 in response to poly(I:C) (Fig. 4). Which of the pathways mainly takes part in IRF-3 activation, what molecule associates with TICAM-1 and NAP1 or RIG-I and NAP1, and whether or not NAP1 is involved in the targeting of viral factors for activation of VAK in any given cell line remain unknown. However, the current literature in this area suggests that the two pathways (TLR3-dependent and -independent), converge on the tri-molecular kinase complex in mDCs (*34*, *35*).

Perspectives—The TLR3-TICAM-1 pathway is intriguing since dsRNA is an essential prerequisite for its activation. TLR3 resides in putative endosomes whereas dsRNA is generated in the cytoplasm during viral replication. How they interact in mDCs and virus-infected cells remains to be investigated. An important issue to be resolved is why this pathway is conserved in mDCs. These cells participate mainly in antigen-presenting and TLR3-mediated IFN-β production. Furthermore, they are

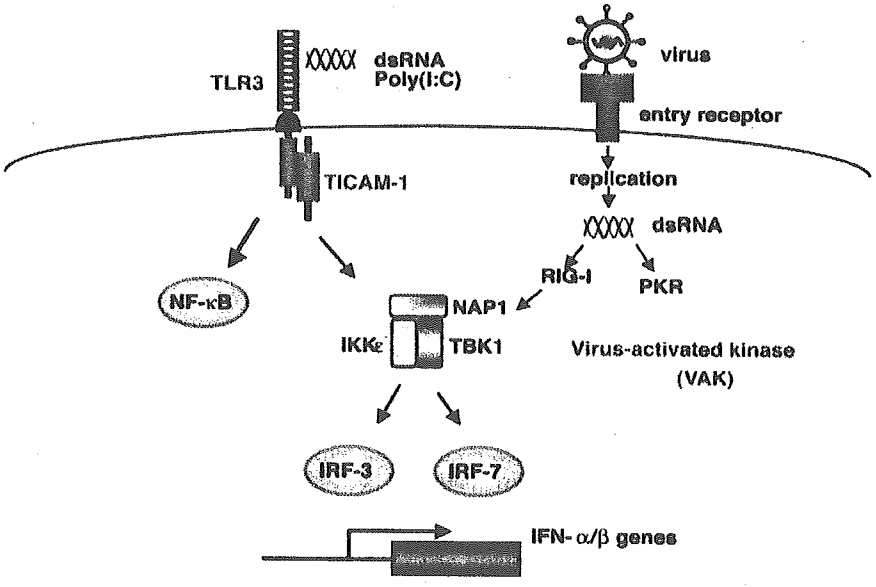

Fig. 4. **The TLR3-TICAM-1 pathway converges with the RIG-I pathway.** The trimolecular complex of NAP1, TBK1 and IKKε is presumed to be virus-activated kinase (VAK), and to be activated via TLR3 and RIG-I in response to dsRNA. TLR3 recognizes dsRNA in certain endosomes in mDCs, whereas RIG-I recognizes it in the cytoplasm (see the text for the differential roles of TLR3 and RIG-I in mDC-mediated antigen-presentation). IRF-7 is an IFN-inducible gene in mDCs (although constitutive in pDCs) and enhances type I IFN production. IFN-β once produced then signals in an auto- or para-cline manner via IFNAR and STAT1/STAT2/IRF-9 to increase up-regulation of CD80/CD86 and CD40. Hence, strong induction of type I IFN and sufficient antigen presentation are accomplished through TICAM-1 signaling in mDCs.

unequivocally involved in cross-priming, an pivotal event for endocytosed antigen presentation via MHC class I in mDCs. Systemic type I IFN production is governed by pDCs via the TLR7/9-MyD88-IRF-7 pathway. Hence, the role of the TLR3-TICAM-1 pathway cannot be simply meant for type I IFN induction alone. Virus-infected apoptotic cells or cell debris may contain viral antigens as well as dsRNA, which can be phagocytosed by mDCs. In such situations, endosomal TLR3 may recognize dsRNA and MHC class II presents the antigen in the phago-endosome. Although the exact molecular mechanism remains to be determined, the endosomal uptake antigen could be followed by class I-restricted CTL induction if co-existing dsRNA activates endosomal TLR3 in mDCs. In fact, OVA-specific $CD8^+$ CTLs are induced via cross-presentation in a TLR3-dependent manner by mouse mDCs ($CD8^+$ splenic DC), which phagocytose poly(I:C) and apoptotic cells (*36*). This, together with a recent review (*37*), allows us to hypothesize that TLR3 and TICAM-1-mediated IRF-3 activation is assigned with cross-priming for class II/class I switching, which might augment antigen presentation in mDCs. This could be the reason for conservation of this pathway in mDCs. Precise comparison of class I antigen presentation and the gene-inducing sequential process in mDCs would allow us to elucidate the role of the TLR3-TICAM-1 pathway in the immune process and its unique function in comparison with the RIG-I pathway. Through such studies, the role of participating cells in infectious lesions, particularly those of mDCs and pDCs, and their subsets, will be clearly revealed. Furthermore, the differential roles played by these agents in a cell-specific manner will be determined at the molecular level.

REFERENCES

1. Takeda, K. (2005) Evolution and integration of innate immune recognition systems: the Toll-like receptors. *J Endotoxin Res.* **11**, 51–55
2. Takeda, K., Kaisho, T., and Akira, S. (2003) Toll-like receptors. *Annu. Rev. Immunol.* **21**, 335–376
3. Jacobs, B. L., and Langland, J. O. (1996) When two strands are better than one: the mediators and modulators of the cellular responses to double-stranded RNA. *Virology* **219**, 339–349
4. Alexopoulou, L., Holt, A. C., Medzhitov, R., and Flavell, R. A. (2001) Recognition of double-stranded RNA and activation of NF-kappaB by Toll-like receptor 3. *Nature* **413**, 732–738
5. Matsumoto, M., Funami, K., Tanabe, M., Oshiumi, H., Shingai, M., Seto, Y., Yamamoto, A., and Seya, T. (2003) Subcellular localization of Toll-like receptor 3 in human dendritic cells. *J. Immunol.* **171**, 3154–3162
6. O'Neill, L. A., Fitzgerald, K. A., and Bowie, A. G. (2003) The Toll-IL-1 receptor adaptor family grows to five members. *Trends Immunol.* **24**, 286–290
7. Seya, T., Oshiumi, H., Sasai, M., Akazawa, T., and Matsumoto, M. (2005) TICAM-1 and TICAM-2: toll-like receptor adapters that participate in induction of type 1 interferons. *Int. J. Biochem. Cell Biol.* **37**, 524–529
8. Honda, K., Yanai, H., Takaoka, A., and Taniguchi, T. (2005) Regulation of the type I IFN induction: a current view. *Int. Immunol.* **17**, 1367–1378
9. Kawai, T., Sato, S., Ishii, K. J., Coban, C., Hemmi, H., Yamamoto, M., Terai, K., Matsuda, M., Inoue, J., Uematsu, S. *et al.* (2004) Interferon-alpha induction through Toll-like receptors involves a direct interaction of IRF7 with MyD88 and TRAF6. *Nat. Immunol.* **5**, 1061–1068
10. Honda, K., Yanai, H., Negishi, H., Asagiri, M., Sato, M., Mizutani, T., Shimada, N., Ohba, Y., Takaoka, A., Yoshida, N. *et al.* (2005) IRF-7 is the master regulator of type-I interferon-dependent immune responses. *Nature* **434**, 772–777
11. Dunne, A., and O'Neill, L. A. (2005) Adaptor usage and Toll-like receptor signaling specificity. *FEBS Lett.* **579**, 3330–3335
12. Barton, G. M., and Medzhitov, R. (2003) Linking Toll-like receptors to IFN-alpha/beta expression. *Nat. Immunol.* **4**, 432–433
13. Fitzgerald, K. A., McWhirter, S. M., Faia, K. L., Rowe, D. C., Latz, E., Golenbock, D. T., Coyle, A. J., Liao, S. M., and Maniatis, T. (2003) IKKepsilon and TBK1 are essential components of the IRF3 signaling pathway. *Nat. Immunol.* **4**, 491–496
14. Sharma, S., tenOever, B.R., Grandvaux, N., Zhou, G.P., Lin, R., and Hiscott, J. (2003) Triggering the interferon antiviral response through an IKK-related pathway. *Science* **300**, 1148–1151

15. Yamamoto, M., Sato, S., Hemmi, H., Hoshino, K., Kaisho, T., Sanjo, H., Takeuchi, O., Sugiyama, M., Okabe, M., Takeda, K. *et al.* (2003) Role of Adaptor TRIF in the MyD88-Independent Toll-Like Receptor Signaling Pathway. *Science* **301**, 640–643
16. Sasai, M., Oshiumi, H., Matsumoto, M., Inoue, N., Fujita, F., Nakanishi, M., and Seya, T. (2005) Cutting Edge: NF-kappaB-activating kinase-associated protein 1 participates in TLR3/Toll-IL-1 homology domain-containing adapter molecule-1-mediated IFN regulatory factor 3 activation. *J. Immunol.* **174**, 27–30
17. Fujita, F., Taniguchi, Y., Kato, T., Narita, Y., Furuya, A., Ogawa, T., Sakurai, H., Joh, T., Itoh, M., Delhase, M. *et al.* (2003) Identification of NAP1, a regulatory subunit of IkappaB kinase-related kinases that potentiates NF-kappaB signaling. *Mol. Cell. Biol.* **23**, 7780–7793
18. Sato, S., Sugiyama, M., Yamamoto, M., Watanabe, Y., Kawai, T., Takeda, K., and Akira, S. (2003) Toll/IL-1 receptor domain-containing adaptor inducing IFN-beta (TRIF) associates with TNF receptor-associated factor 6 and TANK-binding kinase 1, and activates two distinct transcription factors, NF-kappa B and IFN-regulatory factor-3, in the Toll-like receptor signaling. *J. Immunol.* **171**, 4304–4310
19. Jiang, Z., Zamanian-Daryoush, M., Nie, H., Silva, A. M., Williams, B. R., and Li, X. (2003) Poly(I-C)-induced Toll-like receptor 3 (TLR3)-mediated activation of NFkappa B and MAP kinase is through an interleukin-1 receptor-associated kinase (IRAK)-independent pathway employing the signaling components TLR3-TRAF6-TAK1-TAB2-PKR. *J. Biol. Chem.* **278**, 16713–16719
20. Meylan, E., Burns, K., Hofmann, K., Blancheteau, V., Martinon, F., Kelliher, M., and Tschopp, J. (2004) RIP1 is an essential mediator of Toll-like receptor 3-induced NF-kappa B activation. *Nat. Immunol.* **5**, 503–507
21. Pomerantz, J. .L, and Baltimore D. (1999) NF-kappaB activation by a signaling complex containing TRAF2, TANK and TBK1, a novel IKK-related kinase. *EMBO J.* **18**, 6694–6704
22. Peters, R. T., and Maniatis, T. (2001) A new family of IKK-related kinases may function as I kappa B kinase kinases. *Biochim. Biophys. Acta* **1471**, M57–62
23. May, M. J., D'Acquisto, F., Madge, L. A., Glockner, J., Pober, J. S., and Ghosh, S. (2000) Selective inhibition of NF-kappaB activation by a peptide that blocks the interaction of NEMO with the IkappaB kinase complex. *Science* **289**, 1550–1554
24. Hoebe, K., Du, X., Georgel, P., Janssen, E., Tabeta, K., Kim, S. O., Goode, J., Lin, P., Mann, N., Mudd, S. *et al.* (2003) Identification of Lps2 as a key transducer of MyD88-independent TIR signalling. *Nature* **424**, 743–748
25. Wang, T., Town, T., Alexopoulou, L., Anderson, J. F., Fikrig, E., and Flavell, R. A. (2004) Toll-like receptor 3 mediates West Nile virus entry into the brain causing lethal encephalitis. *Nat. Med.* **10**, 1366–1373
26. Guillot, L., Le Goffic, R., Bloch, S., Escriou, N., Akira, S., Chignard, M., and Si-Tahar, M. (2005) Involvement of toll-like receptor 3 in the immune response of lung epithelial cells to double-stranded RNA and influenza A virus. *J. Biol. Chem.* **280**, 5571–5580
27. Li, K., Foy, E., Ferreon, J. C., Nakamura, M., Ferreon, A. C., Ikeda, M., Ray, S. C., Gale, M., Jr., and Lemon, S. M. (2005) Immune evasion by hepatitis C virus NS3/4A protease-mediated cleavage of the Toll-like receptor 3 adaptor protein TRIF. *Proc. Natl. Acad. Sci. USA* **102**, 2992–2997
28. Diebold, S. S., Montoya, M., Unger, H., Alexopoulou, L., Roy, P., Haswell, L. E., Al-Shamkhani, A., Flavell, R., Borrow, P., and Reis e Sousa, C. (2003) Viral infection switches non-plasmacytoid dendritic cells into high interferon producers. *Nature* **424**, 324–328
29. Yoneyama, M., Kikuchi, M., Natsukawa, T., Shinobu, N., Imaizumi, T., Miyagishi, M., Taira, K., Akira, S., and Fujita, T: (2004) The RNA helicase RIG-I has an essential function in double-stranded RNA-induced innate antiviral responses. *Nat. Immunol.* **5**, 730–737
30. Yoneyama, M., Matsumoto, K., Imaizumi, T., Miyagishi, M., Taira, K., Foy, E., Loo, Y-M., Gale, M., Jr., Akira, S., Yonehara, S., Kato, A., and Fujita, T. (2005) Shared and Unique Functions of the DExD/H-Box Helicases RIG-I, MDA5, and LGP2 in Antiviral Innate Immunity. *J. Immunol.* **175**, 2851–2858
31. Horng, T., Barton, G. M., and Medzhitov, R. (2001) TIRAP: an adapter molecule in the Toll signaling pathway. *Nat. Immunol.* **2**, 835–841
32. Shingai, M., Sasai, M., Funami, K., Matsumoto, M., and Seya, T. (2005) NAP1 but not TICAM-1 participates in respiratory syncytial virus (RSV)-mediated interferon induction. *Int. J. Mol. Med.* (in press)
33. Fujita, F., Taniguchi, Y., Kato, T., Narita, Y., Furuya, A., Ogawa, T., Sakurai, H., Joh, T., Itoh, M., Delhase, M. *et al.* (2003) Identification of NAP1, a regulatory subunit of IkappaB kinase-related kinasesthat potentiates NF-kappaB signaling. *Mol. Cell. Biol.* **23**, 7780–7793
34. Seya, T., Akazawa, T., Tsujita, T., and Matsumoto, M. (2006) Role of Toll-like receptors in adjuvant-augmented immunotherapies. *eCAM* (in press) (review)
35. Levy, D. E., and Marie, I. J. (2004) RIGging an antiviral defense–it's in the CARDs. *Nat. Immunol.* **5**, 699–701
36. Schulz, O., Diebold, S. S., Chen, M., Naslund, T. I., Nolte, M. A., Alexopoulou, L., Azuma, Y. T., Flavell, R. A., Liljestrom, P., and Reis e Sousa, C. (2005) Toll-like receptor 3 promotes cross-priming to virus-infected cells. *Nature* **433**, 887–892
37. Schroder, M., and Bowie, A. G. (2005) TLR3 in antiviral immunity: key player or bystander? *Trends Immunol.* **26**, 462–468

FEBS Letters 580 (2006) 93–98

Physical and functional interactions between STAT3 and Kaposi's sarcoma-associated herpesvirus-encoded LANA

Ryuta Muromoto[a,1], Kanako Okabe[a,1], Masahiro Fujimuro[b], Kenji Sugiyama[c], Hideyoshi Yokosawa[b], Tsukasa Seya[d], Tadashi Matsuda[a,*]

[a] Department of Immunology, Graduate School of Pharmaceutical Sciences, Hokkaido University, Sapporo 060-0812, Japan
[b] Department of Biochemistry, Graduate School of Pharmaceutical Sciences, Hokkaido University, Sapporo 060-0812, Japan
[c] Nippon Boehringer Ingelheim Co., Ltd., Kawanishi Pharma Research Institute, 3-10-1 Yato, Kawanishi, Hyogo 666-0193, Japan
[d] Department of Microbiology and Immunology, Graduate School of Medicine, Hokkaido University, Sapporo 060-8638, Japan

Received 22 October 2005; revised 22 November 2005; accepted 23 November 2005

Available online 6 December 2005

Edited by Lukas Huber

Abstract The Kaposi's sarcoma-associated herpesvirus (KSHV)-encoded latency-associated nuclear antigen (LANA) is known to modulate viral and cellular gene expression. We show that LANA directly associates with an interleukin-6 signal transducer, signal transducer and activator of transcription 3 (STAT3) and that LANA enhances the transcriptional activity of STAT3. Coimmunoprecipitation studies documented a physical interaction between LANA and STAT3 in transiently transfected 293T cells as well as the KSHV-infected primary effusion lymphoma (PEL) cell line. Furthermore, small-interfering RNA-mediated reduction of LANA expression decreased the STAT3-dependent transcription in KSHV-positive PEL cells, whereas overexpression of LANA enhanced STAT3 activity in KSHV-negative B lymphoma cells. These data demonstrate that LANA is a transcriptional co-activator of STAT3, and may have implications for the pathogenesis of KSHV-associated diseases.

Keywords: Signal transducer and activator of transcription 3; Kaposi's sarcoma-associated herpesvirus; Latency-associated nuclear antigen; Transcription

1. Introduction

Signal transducer and activator of transcription 3 (STAT3) was originally cloned as an acute-phase response factor activated by interleukin-6 (IL-6) in mouse liver, and also by homology to STAT1 [1,2]. Growth factors, such as epidermal growth factor, platelet-derived growth factor and colony-stimulating factor-1, can also stimulate STAT3 activity [1,2]. STAT3 is also known to play crucial roles in early embryonic development as well as in other biological responses including cell growth and apoptosis [1–3]. Furthermore, STAT3 is constitutively activated in oncogene-transformed cells and various primary tumors and cell lines [4]. Several tumor viruses are also known to be associated with STAT3 activation. STAT3 is constitutively activated in human T cell lymphotrophic virus I-transformed T cells and Epstein–Barr virus (EBV)-related lymphoma cell lines [5–7]. The herpesvirus saimiri tyrosine kinase-interacting protein Tip-484 also activates STAT3 [8].

The Kaposi's sarcoma-associated herpesvirus (KSHV), also known as human herpesvirus 8, has been associated with HIV-related and -unrelated cases of Kaposi's sarcoma, primary effusion lymphoma (PEL), and multicentric Castleman disease [9–11]. The majority of KSHV-infected cells harbor the virus in a latent form. During viral latency, latency-associated nuclear antigen (LANA), is critical to the persistence of KSHV episomes and functions in this capacity by tethering viral episomes to chromosomes during mitosis [12–14]. Viral IL-6, the KSHV homolog of human IL-6, is known to serve as an autocrine growth factor for KSHV-infected PEL cells [15]. Furthermore, STAT3 plays a critical role in promoting survival of KSHV-infected PEL cells [16]. LANA physically interacts with cellular proteins, such as p53, pRB and GSK3β, resulting in inhibition of p53-mediated apoptosis, dysregulation of β-catenin and the Wnt signaling pathway [17–19].

In present study, we examined the physical and functional interactions between STAT3 and LANA in a KSHV-infected PEL cell line. Furthermore, RNA interference and overexpression experiments confirmed that LANA modulates STAT3 activity in the KSHV-infected or -uninfected human B lymphoma cells. Thus, these data show that LANA is a transcriptional co-activator of STAT3.

2. Materials and methods

2.1. Reagents and antibodies

Recombinant human IL-6, interferon (IFN)-β and erythropoietin (EPO) were kindly provided from Ajinomoto (Tokyo, Japan), Sumitomo Pharmaceuticals (Osaka, Japan) and Kirin Company. (Tokyo, Japan), respectively. Recombinant human LIF was purchased from INTERGEN (Purchase, NY). Expression vectors, epitope-tagged STAT3, STAT3YF, STAT3–LUC, STAT3-C, EPO receptor, ISRE–LUC, STAT5–LUC were provided by Dr. T. Hirano (Osaka University, Osaka, Japan), Dr. J.F. Bromberg (Rockefeller University, New York, NY), Dr. J.N. Ihle (St. Jude CRH, Memphis, TN) and Dr. D. Wang (The Blood Res. Inst., Milwaukee, WI), respectively [20,21]. FLAG–LANA (pDY52) and LANA–SiRNAs (siN–LANA and siC–LANA) cloned into pSuper plasmid were previously described [18]. FLAG–LANA deletion mutants were generated by PCR and

*Corresponding author. Fax: +81 11 706 4990.
E-mail address: tmatsuda@pharm.hokudai.ac.jp (T. Matsuda).

[1] These authors contributed equally to this work.

Abbreviations: STAT, signal transducer and activator of transcription; KSHV, Kaposi sarcoma-associated herpesvirus; LANA, latency-associated nuclear antigen; PEL, primary effusion lymphoma

0014-5793/$32.00
doi:10.1016/j.febslet.2005.11.057

sequenced (primer sequences are available upon request). Anti-LANA mAb was purchased from Advanced Biotechnologies Inc. (Maryland USA). Anti-Myc, anti-GST, anti-STAT3, anti-cyclin D1 and anti-cdk4 antibodies were purchased from Santa Cruz Biotechnology (Santa Cruz, CA). Anti-phosphoSTAT3 (Tyr705) was purchased from Cell signaling Technologies (Beverly, MA). Anti-FLAG M2 mAb, rabbit polyclonal anti-FLAG antibody were purchased from Sigma (St. Louis, MO). Fluorescein isothiocyanate (FITC)-conjugated anti-rabbit IgG, rhodamine-conjugated anti-mouse IgG, anti-Actin were purchased from Chemicon (Temecula, CA).

2.2. Cell culture, transfections, and luciferase assays

Human embryonic kidney carcinoma cell line, 293T was maintained in DMEM containing 10% fetal bovine serum (FBS) and transfected by the standard calcium precipitation protocol. Luciferase (LUC) assay was performed as described [22]. Human hepatoma cell line Hep3B was maintained in DMEM containing 10% FBS and transfected with using jetPEI (PolyPlus-transfection, Strasbourg, France) according to the manufacturer's instructions [23]. Before stimulation, the cells were cultured for 12 h in DMEM containing 1% FBS followed by treatment with IL-6.

2.3. Nucreofection and reporter assay of B cells

HBL6 cells ($KSHV^+$, EBV^+) and DG75 cells ($KSHV^-$, EBV^-) were grown in RPMI 1640 medium containing 10% FBS. 5×10^6 of HBL6 (or DG75) cells were nucreofected with 2.5 μg of STAT3–LUC, 0.3 μg of pRL-TK (for internal control) and 2.5 μg of LANA siRNA plasmid (or FLAG–LANA) [19] by Human B Cell Nucleofector Kit (Amaxa biosystems, Cologne, Germany). Cells were resuspended in 0.2 ml of lysis solution, passive lysis buffer (Promega, Madison, WI) for LUC assay.

2.4. Immunoprecipitation, immunoblotting and indirect immunofluorescence

Immunoprecipitation, Western blotting and indirect immunofluorescence were performed as described previously [24].

3. Results and discussion

3.1. STAT3 and LANA physically interact in vivo

IL-6/STAT3 signaling has been documented to play crucial roles in the development of the KSHV-associated diseases [15,16]. These facts led us to examine the molecular interactions between an IL-6 signaling molecule, STAT3 and a most abundant latent protein, LANA in KSHV-infected cells. We first examined whether LANA physically interacts with STAT3. To demonstrate in vivo binding of LANA to STAT3, we performed coimmunoprecipitation studies in 293T cells that were transiently transfected with FLAG–LANA and Myc–STAT3 expression constructs. The transfected 293T cells were lysed and subjected to immunoprecipitation with anti-FLAG antibody. Immunoprecipitates were then used in Western blot analysis with anti-Myc antibody. As shown in Fig. 1A, STAT3 interacted with LANA in 293T cells. To further establish the relevance of the interaction between endogenous LANA and STAT3, we performed co-immunoprecipitation studies on the KSHV-positive BC3 PEL cell line. In KSHV-positive PEL cells but not negative B lymphoma cells, STAT3 was constitutively tyrosine-phosphorylated (data not shown). Immunoprecipitates with anti-STAT3, but not control IgG, successfully pulled down LANA as demonstrated by Western blotting with an anti-LANA antibody (Fig. 1B). Similar immunoprecipitation studies on KSHV-negative B lymphoma DG75 cells as well as immunoprecipitation with an IgG control antibody, served as negative controls (Fig. 1B).

To next delineate the domains in the LANA that mediate the protein–protein interactions between LANA and STAT3, co-immunoprecipitation experiments were performed with a series of mutant LANA proteins (Fig. 1C). As shown in Fig. 1D (left panels), Deletion of LANA central repeat domain (LANA-NC, Δ332–931) and the C-terminal domain of LANA (LANA-C, 932–1162) interacted with STAT3, whereas the N-terminal domain of LANA (LANA-N, 1–331) failed to interact with STAT3. These data suggest that the C-terminal domain is required for LANA to interact with STAT3.

To characterize further the nature of the interaction between STAT3 and LANA, we attempted to determine where this interaction occurs in cells. LANA localized in the nucleus in the presence or absence of IL-6-stimulation, while IL-6 stimulation induced translocation of STAT3 into nucleus in Hep3B cells (Fig. 1E). The cytoplasmic STAT3 did not co-localize with LANA. However, after IL-6 stimulation, STAT3 translocated into nucleus and co-localized with LANA (Fig. 1D). Consistent with the in vivo interaction data presented above, these results suggest that the activated STAT3 interacts with LANA in the nucleus.

3.2. LANA augments transcriptional activation of STAT3 in 293T cells

To assess the functional relevance between LANA and STAT3, we tested whether LANA affects STAT3-mediated transcriptional activation using transient transfection experiments in 293T cells. The STAT3-mediated transcriptional responses were measured by using STAT3–LUC, in which the α2-macroglobulin promoter drives expression of the LUC reporter gene [20]. 293T cells were transfected with STAT3–LUC together with or without LANA, and treated with LIF and LUC activities were determined. When cells were co-transfected with LANA, the transcriptional activation of STAT3–LUC augmented in a dose-dependent manner (Fig. 2A). Co-expression of a dominant negative STAT3, STAT3YF inhibited LANA-mediated augmentation of STAT3 activation, suggesting that LANA affected the STAT3-mediated transcriptional activity. To next assess the direct interaction between STAT3 and LANA, we used a constitutively active form of STAT3, STAT3-C [21]. 293T cells were transfected with STAT3–LUC and expression vectors for LANA and/or STAT3–C. As shown in Fig. 2B, STAT3–LUC activation by STAT3–C was augmented by LANA in a dose dependent manner. We also tested whether LANA induces IL-6 mRNA in 293T cells by RT-PCR. However, any IL-6 mRNA expression was observed after LANA expression in 293T cells (data not shown). We next examined the effects of LANA on the IFN-β-induced STAT1 and EPO-induced STAT5 activation using similar transient transfection experiments. However, LANA affected neither STAT1 nor STAT5 activation (Fig. 2C and D). These results indicate that LANA activates STAT3 transcriptional activity but not STAT1 and STAT5, suggesting LANA acts on STAT3 in a specific manner. To further understand the molecular mechanisms responsible for LANA-mediated enhanced STAT3 activation, we examined whether LANA expression affects phopshorylation, dimerization, nuclear translocation/retention or DNA binding activity of STAT3, however, we could not observe any significant effect on these issues by LANA expression in 293T cells (data not shown). We also examined whether LANA physically interacts with unphosphorylated STAT3, such as STAT3YF. In 293T

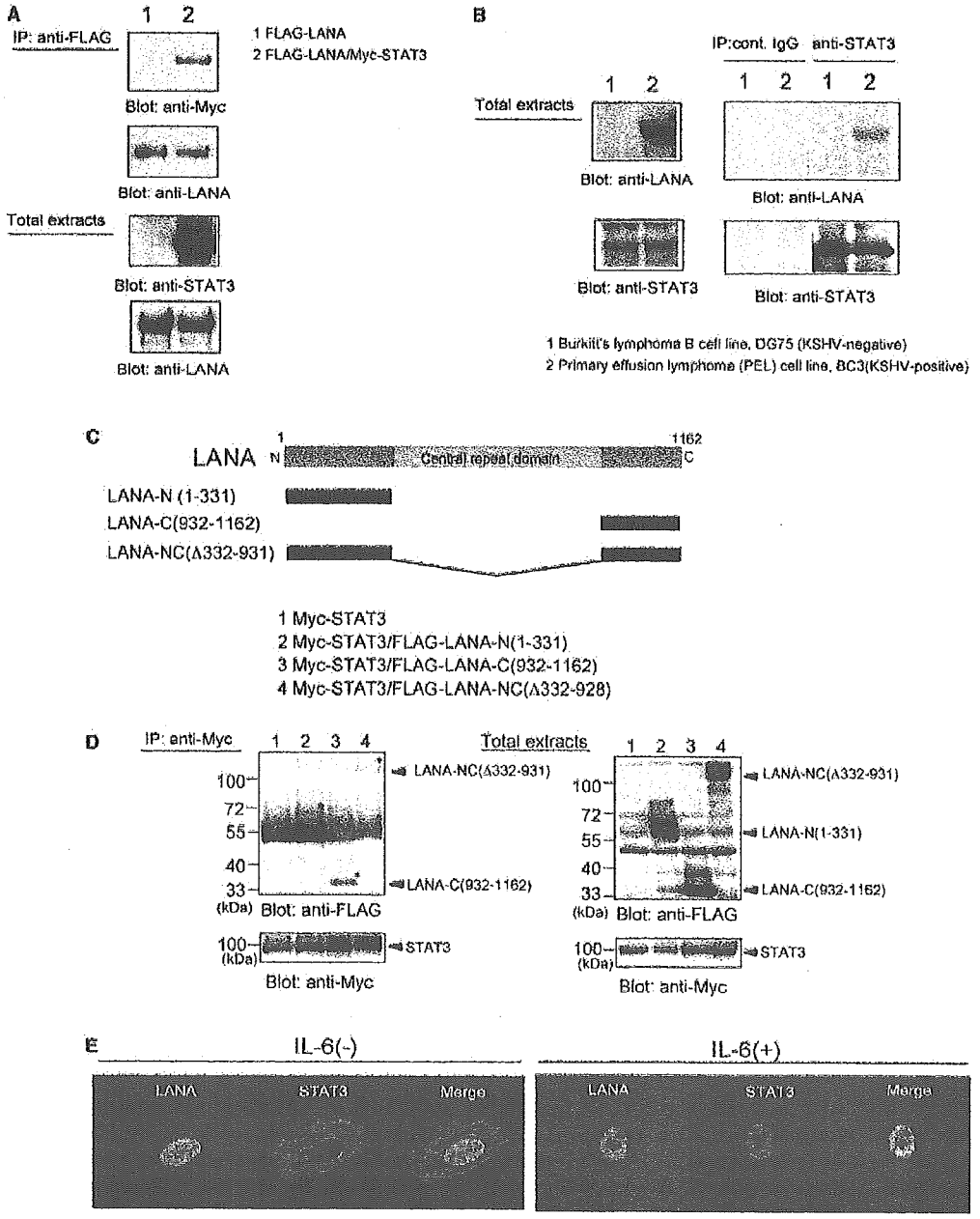

Fig. 1. STAT3 and LANA physically interact in vivo. (A) 293T cells (1×10^7 cells) were transfected with FLAG–LANA (20 μg) together with or without Myc–STAT3 (10 μg). Forty-eight hours after transfection, the cells were lysed, and immunoprecipitated with anti-FLAG antibody and immunoblotted with anti-Myc (upper panel) or anti-LANA antibody (middle panel). Total cell lysates (1%) were blotted with anti-Myc or anti-LANA antibody (lower panels). (B) Human Burkitt's lymphoma DG75 (KSHV-negative) or primary effusion lymphoma (PEL) BC3 (KSHV-positive) cells (2×10^7) were lysed, and immunoprecipitated with control IgG or anti-STAT3 antibody and immunoblotted with anti-LANA antibody (upper panels) or anti-STAT3 antibody (lower panels). (C) Domain structure of LANA and mutant fragments are schematically shown. (D) 293T cells (1×10^7 cells) were transfected with Myc–STAT3 (10 μg) together with or without LANA-N (1–331), LANA-C (932–1162) and LANA-NC (Δ332–931) (10 μg). Forty-eight hours after transfection, the cells were lysed, immunoprecipitated with anti-Myc antibody and immunoblotted with anti-FLAG or anti-Myc antibody (left panels). Total cell lysates (1%) were blotted with anti-FLAG or anti-Myc antibody (right panels) to monitor the expression of LANA or STAT3 proteins. The asterisks indicate the migration position of LANA mutants. (E) Hep3B cells were transfected with Myc–STAT3 (1 μg) and FLAG–LANA (1 μg). Thirty hours after transfection, cells were treated with or without IL-6 (100 ng/ml) for 40 min, and then fixed and reacted with rabbit anti-FLAG polyclonal and mouse anti-Myc monoclonal antibody and visualized with FITC-conjugated anti-rabbit antibody or rhodamine-conjugated anti-mouse IgG antibody.

cells, we could detect a direct interaction between LANA and STAT3YF (data not shown), suggesting that phosphorylation of STAT3 may be not necessary for their physical interactions.

However, LANA-mediated enhanced STAT3 activation was observed only after LIF stimulation. These results indicate that STAT3 can interact with LANA in the nucleus after its

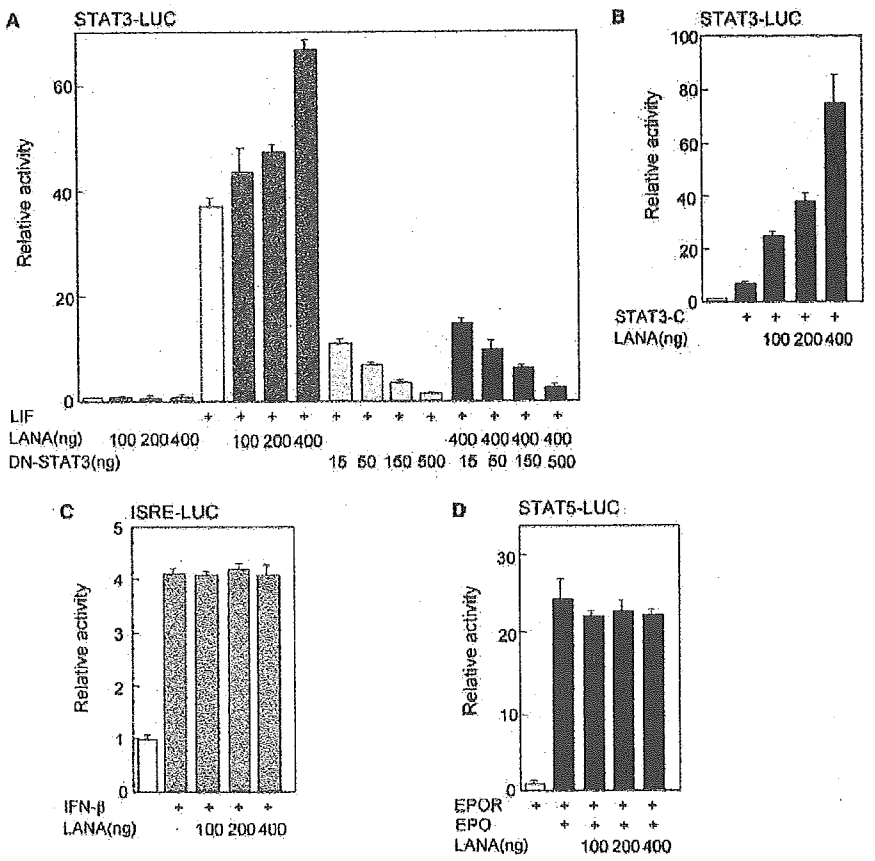

Fig. 2. LANA augments transcriptional activation of STAT3 in 293T cells. (A) 293T cells in a 12-well plate were transfected with STAT3–LUC (0.2 μg) and/or indicated amounts of empty vector, expression vector for LANA or STAT3YF. Thirty-six hours after transfection, the cells were stimulated with LIF (100 ng/ml) for additional 12 h. The stimulated cells were harvested, and LUC activities were measured. (B) 293T cells in a 12-well plate were transfected with STAT3–LUC (0.2 μg) together with or without STAT3-C (500 ng) and/or indicated amounts (100–400 ng) of expression vector for LANA. Forty eight hours after transfection, the cells were harvested, and LUC activities were measured. (C) 293T cells in a 12-well plate were transfected with ISRE–LUC (0.4 μg) and/or indicated amounts (100–400 ng) of expression vector for LANA. Thirty-six hours after transfection, the cells were stimulated with IFN-β (50 U/ml) for additional 8 h. The stimulated cells were harvested, and LUC activities were measured. (D) 293T cells in a 12-well plate were transfected with STAT5–LUC (0.4 μg) together with EPO receptor (0.05 μg) and/or indicated amounts (100–400 ng) of expression vector for LANA. Thirty-six hours after transfection, the cells were stimulated with EPO (0.03 U/ml) for additional 12 h. The stimulated cells were harvested, and LUC activities were measured. The above results are indicated as fold induction of LUC activity from triplicate experiments, and the error bars represent the S.D.

phosphorylation and translocation. Further detailed work will be required to clarify the molecular mechanisms of LANA-mediated enhancement of STAT3 activation.

3.3. LANA acts as a transcriptional activator for STAT3 in B cells

To understand the physiology of molecular interactions between STAT3 and LANA, we further examined the effects of LANA gene silencing on STAT3 activity in KSHV-infected PEL cells. We co-transfected STAT3–LUC construct with the LANA or control siRNA into HBL6 cells and assessed reporter gene expression. LANA siRNA reduced expression of cellular LANA expression by about 50% compared to control siRNA (Fig. 3A). Importantly, the LANA siRNA markedly reduced the STAT3 target gene expression, such as cyclin D1 and cdk4 [21] as well as the reporter gene expression from the STAT3–LUC construct compared to the control siRNA, although the phosphorylation level of STAT3 did not alter by treatment of LANA siRNA (Fig. 3A). To further confirm the enhanced effect of LANA on STAT3 activation, we overexpressed LANA together with the STAT3–LUC construct in a KSHV-negative DG75 cells. As shown in Fig. 3B, ectopically expressed LANA markedly augmented STAT3–LUC in DG75 cells. These data indicate that LANA plays a critical role in the enhanced STAT3 activation in KSHV-infected PEL cells.

3.4. Concluding remarks

STAT3 is constitutively phosphorylated and activated in various primary human tumors and in transformed cell lines and is implicated in tumorigenesis [2–4]. However, molecular mechanisms of the persistent activation of STAT3 in human tumor cells are largely unknown. Recently, the hepatitis C virus (HCV) core protein has been shown to directly interact with and activate STAT3 through phosphorylation of the critical tyrosine residue [25]. Chronic infection by HCV is known to associate with development of liver cirrhosis and hepatocellular carcinoma. HCV core protein is also proposed to be involved in the virus-induced transformation, indicating that the HCV core protein cooperates with STAT3, which leads to cellular transformation.

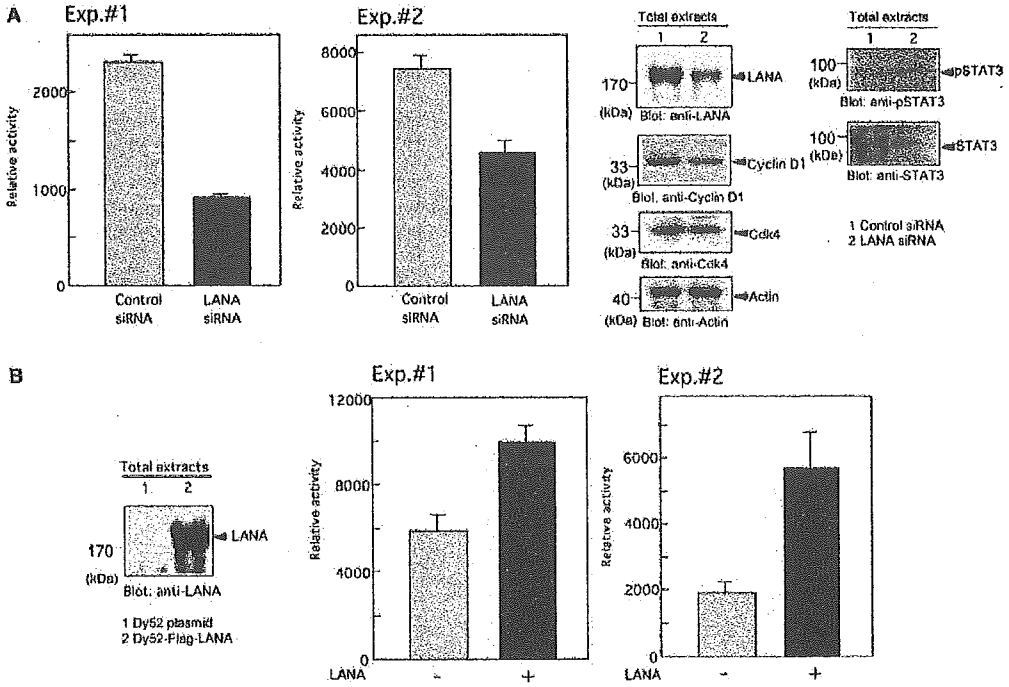

Fig. 3. LANA acts as a transcriptional activator for STAT3 in B cells. (A) To abolish expression of endogenous LANA and measure LUC activities from STAT3 signaling, HBL6 cells were nucreofected with 2.5 μg of LUC reporter (STAT3–LUC), 0.3 μg of pRL-TK and and 2.5 μg of LANA siRNA expressing plasmid (1.25 μg of siN–LANA and 1.25 μg of siC–LANA) or 2.5 μg of control siRNA plasmid by nucreofection with Human B Cell Nucleofector Kit according to their optimized protocol. Cells were harvested after 2 (Exp. #2) and 3 days (Exp. #1) and resuspended in 0.2 ml of lysis solution for LUC assay. One part of lysate was subjected to Western blotting analysis using anti-LANA rat mAb to confirm the knock down of LANA expression. The same samples were also subjected to Western blotting analysis using anti-phosphoSTAT3 (Tyr705), anti-STAT3, anti-cyclin D1 or anti-cdk4 antibodies. (B) DG75 cells were nucreofected with 2.5 μg of STAT3–LUC, 0.3 μg of pRL-TK and 2.5 μg of FLAG–LANA by nucleofector as well as HBL6 and cells were harvested after 5 (Exp. #1) and 6 days (Exp. #2). Nucreofection was done with a total of 5 μg of DNA (adjusted with vector plasmid as a carrier) per each sample. Cells lysate were subjected to LUC assay and Western blotting with anti-LANA rat mAb.

In this study, we propose a novel interaction between STAT3 and the KSHV-derived LANA in PEL cells. LANA augmented transcriptional activity of STAT3 in 293T cells. Furthermore, small-interfering RNA-mediated reduction of LANA expression decreased the STAT3-dependent transcription in KSHV-positive PEL cells, whereas overexpression of LANA enhanced STAT3 activity in KSHV-negative B cells. Thus, further understanding of the detailed molecular interactions between STAT3 and LANA may provide a novel therapeutic strategy for the KSHV-associated tumors.

References

[1] Ihle, J.N. (1996) STATs: signal transducers and activators of transcription. Cell 84, 331–334.
[2] Hirano, T., Ishihara, K. and Hibi, M. (2000) Roles of STAT3 in mediating the cell growth, differentiation and survival signals relayed through the IL-6 family of cytokine receptors. Oncogene 19, 2548–2556.
[3] Levy, D.E. and Lee, C.K. (2002) What does Stat3 do? J. Clin. Invest. 109, 1143–1148.
[4] Bowman, T., Garcia, R., Turkson, J. and Richard Jove, R. (2000) STATs in oncogenesis. Oncogene 19, 2474–2488.
[5] Migone, T.S., Lin, J.X., Cereseto, A., Mulloy, J.C., O'Shea, J.J., Franchini, G. and Leonard, W.J. (1995) Constitutively activated Jak-STAT pathway in T cells transformed with HTLV-I. Science 269, 79–81.
[6] Weber-Nordt, R.M., Egen, C., Wehinger, J., Ludwig, W., Gouilleux-Gruart, V., Mertelsmann, R. and Finke, J. (1996) Constitutive activation of STAT proteins in primary lymphoid and myeloid leukemia cells and in Epstein-Barr virus (EBV)-related lymphoma cell lines. Blood 88, 809–816.
[7] Chen, H., Lee, J.M., Zong, Y., Borowitz, M., Ng, M.H., Ambinder, R.F. and Hayward, S.D. (2001) Linkage between STAT regulation and Epstein–Barr virus gene expression in tumors. J. Virol. 75, 2929–2937.
[8] Lund, T.C., Garcia, R., Medveczky, M.M., Jove, R. and Medveczky, P.G. (1997) Activation of STAT transcription factors by herpesvirus Saimiri Tip-484 requires p56lck. J. Virol. 71, 6677–6682.
[9] Chang, Y., Cesarman, E., Pessin, M.S., Lee, F., Culpepper, J., Knowles, D.M. and Moore, P.S. (1994) Identification of herpesvirus-like DNA sequences in AIDS-associated Kaposi's sarcoma. Science 266, 1865–1869.
[10] Moore, P.S. and Chang, Y. (1995) Detection of herpesvirus-like DNA sequences in Kaposi's sarcoma in patients with and without HIV infection. N. Engl. J. Med. 332, 1181–1185.
[11] Soulier, J., Grollet, L., Oksenhendler, E., Cacoub, P., Cazais-Hatem, D., Babinet, P., d'Agay, M.-F., Clauvel, J.-P., Raphael, M., Degos, L. and Sigaux, F. (1995) Kaposi's sarcoma-associated herpesvirus-like DNA sequences in multicentric Castleman's disease. Blood 86, 1276–1280.
[12] Zhong, W., Wang, H., Herndier, B. and Ganem, D. (1996) Restricted expression of Kaposi sarcoma-associated herpesvirus (human herpesvirus 8) genes in Kaposi sarcoma. Proc. Natl. Acad. Sci. USA 93, 6641–6646.
[13] Sarid, R., Flore, O., Bohenzky, R.A., Chang, Y. and Moore, P.S. (1998) Transcription mapping of the Kaposi's sarcoma-associated herpesvirus (human herpesvirus 8) genome in a body cavity-based lymphoma cell line (BC-1). J. Virol. 72, 1005–1012.
[14] Ballestas, M.E., Chatis, P.A. and Kaye, K.M. (1999) Efficient persistence of extrachromosomal KSHV DNA mediated by latency-associated nuclear antigen. Science 284, 641–644.

[15] Miles, S.A., Rezai, A.R., Salazar-Gonzalez, J.F., Meyden, M.V., Stevens, R.H., Logan, D.M., Mitsuyasu, R.T., Taga, T., Hirano, T., Kishimoto, T. and Martinez-Maza, O. (1990) AIDS Kaposi sarcoma-derived cells produce and respond to interleukin 6. Proc. Natl. Acad. Sci. USA 87, 4068–4072.
[16] Aoki, Y., Feldman, G.M. and Tosato, G. (2003) Inhibition of STAT3 signaling induces apoptosis and decreases survivin expression in primary effusion lymphoma. Blood 101, 1535–1542.
[17] Friborg, J., Kong, W., Hottiger, M.O. and Nabel, G.J. (1999) p53 inhibition by the LANA protein of KSHV protects against cell death. Nature 402, 889–894.
[18] Radkov, S.A., Kellam, P. and Boshoff, C. (2000) The latent nuclear antigen of Kaposi sarcoma-associated herpesvirus targets the retinoblastoma-E2F pathway and with the oncogene Hras transforms primary rat cells. Nat. Med. 6, 1121–1127.
[19] Fujimuro, M., Wu, F.Y., ApRhys, C., Kajumbula, H., Young, D.B., Hayward, G.S. and Hayward, S.D. (2003) A novel viral mechanism for dysregulation of beta-catenin in Kaposi's sarcoma-associated herpesvirus latency. Nat. Med. 9, 300–306.
[20] Nakajima, K., Yamanaka, Y., Nakae, K., Kojima, H., Ichiba, M., Kiuchi, N., Kitaoka, T., Fukada, T., Hibi, M. and Hirano, T. (1996) A central role for Stat3 in IL-6-induced regulation of growth and differentiation in M1 leukemia cells. EMBO J. 15, 3651–3658.
[21] Bromberg, J.F., Wrzeszczynska, M.H., Devgan, G., Zhao, Y., Pestell, R.G., Albanese, C. and Darnell, J.E. (1999) Stat3 as an oncogene. Cell 98, 295–303.
[22] Sekine, Y., Yamamoto, T., Yumioka, T., Sugiyama, K., Tsuji, S., Oritani, K., Shimoda, K., Minoguchi, M., Yoshimura, A. and Matsuda, T. (2005) Physical and functional interactions between STAP-2/BKS and STAT5. J. Biol. Chem. 280, 8188–8196.
[23] Imoto, S., Sugiyama, K., Muromoto, R., Sato, N., Yamamoto, T. and Matsuda, T. (2003) Regulation of transforming growth factor-beta signaling by protein inhibitor of activated STAT, PIASy through Smad3. J. Biol. Chem. 278, 34253–34258.
[24] Muromoto, R., Sugiyama, K., Takachi, A., Imoto, S., Sato, N., Yamamoto, T., Oritani, K., Shimoda, K. and Matsuda, T. (2004) Physical and functional interactions between Daxx and DNA methyltransferase 1-associated protein, DMAP1. J. Immunol. 172, 2985–2993.
[25] Yoshida, T., Hanada, T., Tokuhisa, T., Kosai, K., Sata, M., Kohara, M. and Yoshimura, A. (2002) Activation of STAT3 by the hepatitis C virus core protein leads to cellular transformation. J. Exp. Med. 196, 641–653.

J. Biochem. **137**, 339–347 (2005)
DOI: 10.1093/jb/mvi042

Rational Design of Dual-Functional Aptamers That Inhibit the Protease and Helicase Activities of HCV NS3

Takuya Umehara[1,2], Kotaro Fukuda[1,2], Fumiko Nishikawa[1], Michinori Kohara[3], Tsunemi Hasegawa[2] and Satoshi Nishikawa[1,*]

[1]Institute for Biological Resources and Functions, National Institute of Advanced Industrial Science and Technology (AIST), Tsukuba, Ibaraki 305-8566; [2]Department of Material and Biological Chemistry, Faculty of Science, Yamagata University, Yamagata 990-8560; and [3]Tokyo Metropolitan Institute of Medical Science, Bunkyo-ku, Tokyo 113-8613

Received November 24, 2004; accepted December 26, 2004

The hepatitis C virus (HCV) non-structural protein 3 (NS3) is a multifunctional enzyme with protease and helicase activities. It is essential for HCV proliferation and is therefore a target for anti-HCV drugs. Previously, we obtained RNA aptamers that inhibit either the protease or helicase activity of NS3. During the present study, these aptamers were used to create advanced dual-functional (ADD) aptamers that were potentially more effective inhibitors of NS3 activity. The structural domain of the helicase aptamer, #5Δ, was conjugated *via* an oligo(U) tract to the 3′-end of the dual functional aptamer NEO-III-14U or the protease aptamer G9-II. The spacer length was optimized to obtain two ADD aptamers, NEO-35-s41 and G925-s50; both were more effective inhibitors of NS3 protease/helicase activity *in vitro*, especially the helicase, with a four- to five-fold increase in inhibition compared with #5 and NEO-III-14U. Furthermore, G925-s50 effectively inhibited NS3 protease activity in living cells and HCV replication *in vitro*. Overall, we have demonstrated rational RNA aptamer design based on features of both aptamer and target molecules, as well as successfully combining aptamer function and increasing NS3 inhibition.

Key words: hepatitis C virus, NS3 helicase, NS3 protease, RNA aptamer, RNA design.

The hepatitis C virus (HCV) is the major etiological agent of non-A, non-B hepatitis, with a worldwide carriage rate of 3%. Most patients develop chronic hepatitis, and persistent infection often leads to liver cirrhosis or hepatocellular carcinoma. Recently, combination therapy with interferon and ribavirin has been found to be most effective against HCV. However, not all subtypes respond to treatment, and the drugs can cause serious side effects (*1*). The development of anti-HCV drugs with greater safety and efficacy is therefore a priority.

HCV is a single-stranded RNA virus that belongs to the *Flaviviridae* family (*2*). The ~9.6-kb genome with positive polarity encodes a precursor polyprotein (~3,010 amino acids) that is processed to structural (core protein C, and envelope glycoproteins E1 and E2) and non-structural (NS2, NS3, NS4A, NS4B, NS5A and NS5B) proteins by a host signal peptidase and two viral proteases, NS2-3 and NS3 (*3*). The NS3 protein is a multi-functional enzyme with a trypsin-like protease within the amino (N)-terminal one-third, and an NTP-dependent RNA/DNA helicase in the remaining two-thirds (*4–6*). It is generally accepted that the protease domain cleaves the junctions between the non-structural proteins, together with cofactor NS4A (*7*). The helicase domain unwinds the double-stranded RNA generated by the RNA-dependent RNA polymerase NS5B during genome replication (*8*, *9*). As NS3 is essential for HCV replication and proliferation, new anti-HCV drugs could potentially be directed against this protein (*10*, *11*).

Previously, we used *in vitro* selection to obtain aptamers with activity against the NS3 protease or helicase domain. The aptamers G9-I, -II and -III bound specifically to the protease domain and strongly inhibited its activity (*12*). Functional and structural analysis of the major clone aptamer G9-I allowed a minimized aptamer, ΔNEO-III, to be constructed (*13*). The three G9 aptamers were transfected into cultured cells where G9-II showed the most efficient NS3 protease-inhibitory activity (*14*, *15*). NS3 has been reported to bind preferentially to the poly(U) sequence at the (+) 3′-untranslated region (UTR) of the HCV genome (*16*, *17*). We previously tested the effect of adding an oligo(U) 14-mer to the 3′-end of ΔNEO-III (NEO-III-14U). This produced a dual-functional aptamer causing both NS3 protease and helicase inhibition (*18*). The introduction of the oligo(U) tail not only increased binding and protease inhibition, but also resulted in an additional helicase-inhibitory activity. It has also been reported that the anti-helicase aptamer "#5" binds strongly and inhibited this enzyme. Aptamer #5 comprises a 5′ single-stranded region that interacts with a cleft in the NS3 helicase domain, and a 3′-region with a conserved stem–loop structure that prevents NS3 sliding along single-stranded region of #5. It was thought that aptamer #5 traps NS3 and acts as a substitute for the HCV genomic RNA (*19*).

The aim of the present study was to develop a novel aptamer with enhanced dual-inhibitory activities for the protease and helicase functions of NS3. We rationally

*To whom correspondence should be addressed. Tel: +81-298-61-6085, Fax: +81-298-61-6159, E-mail: satoshi-nishikawa@aist.go.jp

designed advanced dual-functional (ADD) aptamers by fusing previous aptamers with known anti-protease and anti-helicase activities. The ADD aptamers were then characterized in detail using *in vitro* and cell-culture assays. This approach was successful for the rational design of aptamers with enhanced inhibitory activity toward HCV NS3.

MATERIALS AND METHODS

Design and Construction of ADD Aptamers—Two types of ADD aptamer, NEO-35-sX (introduced 8–50-mer spacer) and G925-sX (introduced 5–50-mer spacer), were designed, and their secondary structures were confirmed using the Mulfold program, which is based on the Zuker algorithm (*20*). First, we constructed longer spacer aptamers (>31-mer) using six primers; 5′-AGTAATACGACTCACTATAGGGAGAACCAGCTGGTTT-3′ and 5′-$(A)_{20}$AGGAGAGAGGAAGG-3′ were used for the NEO-35 type, 5′-AGTAATACGACTCACTATAGGGAGAATTCCGACCAGAAG-3′ and 5′-$(A)_{20}$AGAAGAGGAAGGAGAGAGGA-3′ were used for the G925 type and 5′-$(T)_{25}$GGGGACGGAGCCCTTAATG-3′ and 5′-TGGCTGCGCGTCATG-3′ were used for #5Δ. The homopolymeric tracts A_{20} or T_{25} were introduced by PCR to the 3′-end of NEO-III-14U and G9-II, or the 5′-end of #5Δ template DNA (Ex-Taq, Takara). The products were used as overlapping primers in a second PCR. Conjugated aptamers with spacers of various length (31–50-mer) were obtained randomly, and clones NEO-35-s31, -s41 and -s50, and G925-s32, -s40 and -s50, were selected. Additionally G9-II-20U was constructed by cloning the fist PCR product of G9-II type.

Aptamers with shorter spacers, NEO-35-s8 and -s15, and G925-s5 and -s15, were constructed using the same procedure with spacer-length primers; 5′-CGTCCCCAAAAAAAAAGGAGAGAGGAAAGGTAGTC-3′ (for NEO-35-s8), 5′-CGTCCCCAAAAAAAAAAAAAAAAAGGAGAGAGGAAAGGTAG-3′ (for NEO-35-s15), 5′-CTCCGTCCCCAAAAAAGGAGAGAGGAAAGGGTCCC-3′ (for G925-s5) and 5′-CGTCCCCAAAAAAAAAAAAAAAAGGAGAGAGGAAAGGGTC-3′ (for G925-s15).

RNA was transcribed from the DNA templates using an Ampliscribe T7 transcription kit (Epicentre) and purified by electrophoresis through a 7 M urea 8% polyacrylamide denaturing gel.

Expression and Purification of NS3 Protein—The expression plasmid (pT7/His-NS3) containing full-length HCV-NS3 with a His-tag fused to the N-terminus was constructed previously (*19*). *Escherichia coli* strain BL21 (DE3) was transformed with the plasmid, and recombinant NS3 was expressed and purified. *E. coli* cells were pre-cultivated in 20 ml LB medium overnight at 37°C. The culture was added to 1 liter LB medium and grown continuously at 30°C for 12 h without IPTG induction. The cells were harvested and resuspended in lysis buffer [20 mM Tris-HCl (pH 7.6), 500 mM NaCl and 5 mM imidazol]. After sonication, the lysate containing NS3 was loaded onto a Ni-NTA column (Amersham). The column was washed with PBS [20 mM PBS (pH 7.4) and 500 mM NaCl] containing 60 mM imidazol, and the bound proteins were eluted with PBS containing 100 mM and then 200 mM imidazol. The fractions containing NS3 were monitored using SDS-PAGE, pooled and then dialyzed against TNE [10 mM Tris-HCl (pH 7.6), 50 mM NaCl and 1 mM EDTA]. After microcon concentration YM-50 (Millipore), the NS3 was stored at –20°C mixed with an equal volume of glycerol (0.5× TNE and 50% glycerol).

NS3 Protease-Inhibition Assay—The protease-inhibition assay was similar to that reported previously (*12*). A dansyl-labeled synthetic peptide substrate (NS5A/5B junction sequence, 17-mer amino acid, 43 μM) was added to the premixture [50 mM Tris-HCl (pH 7.8), 5 mM $MgCl_2$, 5 mM $CaCl_2$, 10 mM DTT, 1.2 μM NS3, 13.5 μM NS4A cofactor peptide and various concentrations of aptamers]. The cleavage reaction was incubated at 25°C for 60 min, and then stopped by adding NaOH to a final concentration of 0.4 M. The reaction products were separated by reverse-phase HPLC (TSK gel ODS-120T) and the cleavage efficiency was quantitated. The assay mixture in the presence of 3 mM ATP was incubated at 37°C for 20 min and analyzed as described above.

NS3 Helicase-Inhibition Assay—The helicase-inhibition assay was carried out as reported previously (*18*). A partial duplex DNA substrate (0.13 nM), comprising a 5′-^{32}P–labeled DNA oligonucleotide (n = 30) annealed to bacteriophage M13mp18(+) ssDNA, was added to the premixture [25 mM MOPS-NaOH (pH 7.0), 2.5 mM DTT, 100 μg/ml BSA, 5 mM $MgCl_2$, 5 mM $CaCl_2$, 3 mM ATP and 100 nM NS3] and aptamers at various concentrations. The unwinding reactions were incubated at 37°C for 30 min, then stopped by adding 5 μl stop solution [0.1 M Tris-HCl (pH 7.6), 20 mM EDTA, 0.5% SDS, 0.1% nonidet P40, 0.1% bromophenol blue 0.1% xylene cyanol and 25% glycerol]. The reaction products were loaded onto an 8% native polyacrylamide gel containing 0.5× TBE, and unwinding activity was analyzed using a BAS2500 (Fuji Film).

Filter-Binding Assay—The filter-binding assay for NEO-35-s41 or G925-s50 and NS3 was performed using the same conditions as for the helicase assay, but ATP was omitted. NS3 (0.032–500 nM) was added to the reaction mixture, which contained internal labeled aptamers (5 nM). The binding reactions were incubated at 37°C for 30 min and passed through an MF™-membrane filter 0.45 μm HA (Millipore). The membrane was washed immediately with 1 ml of binding buffer without ATP, and the radioisotope activity on the membrane was counted using a BAS2500. The relative binding ratio was calculated, and the binding parameters [maximum binding (B_{max}), the equilibrium-dissociation constant (K_d) and the Hill coefficient (n_H)] were analyzed using a non-linear curve fitting the following equation: binding (%) = $100 \times B_{max}[NS3]^n/(K_d + [NS3]^n)$.

UV Cross-Linking and Electrophoretic Mobility-Shift Analysis (EMSA)—The reaction mixture used to perform UV cross-linking (10 μl) contained 0.2 μM ^{32}P-internal labeled NEO-35-s41 or G925-s50 in 25 mM MOPS-NaOH (pH 7.0), 2.5 mM DTT, 100 μg/ml BSA, 5 mM $MgCl_2$, 5 mM $CaCl_2$ and 2 μM NS3. The reaction was incubated at room temperature for 30 min and then exposed to UV irradiation (254 nM) for 30 min using a transilluminator (Mineralight UVGL-57) from a distance of 3 cm. The cross-linked samples were separated by electrophoresis through a gradient SDS polyacrylamide gel (4–20%; SuperSep, Wako) and detected using a BAS2500. The

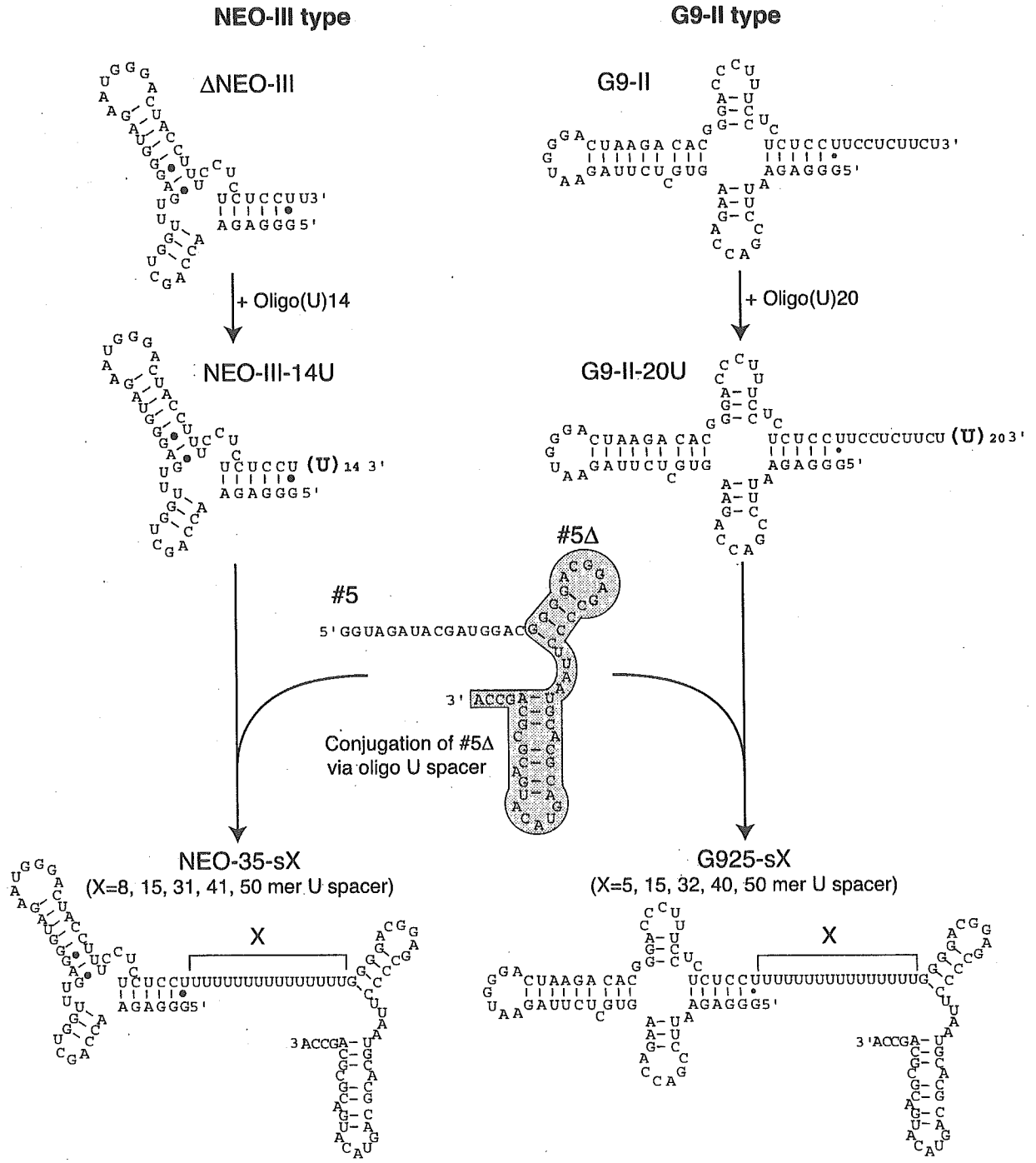

Fig. 1. **Design and construction of two types of conjugated aptamers, NEO-35-sX and G925-sX (X indicates spacer length).** They were conjugated with #5Δ (gray area), which is the structural domain of the helicase aptamer #5, at the 3′-end of the protease aptamer NEO-III-14U or G9-II *via* an oligo(U) spacer (5–50-mer). The protease aptamer, NEO-III-14U, was identified in our recent report (*18*). G9-II-20U has a 20-mer oligo(U) stretch introduced at the 3′-end of G9-II and in the middle of the G925-sX construction. Secondary structures were predicted using the Mulfold program.

molecular weight was estimated by comparison to precision-plus protein standards (Bio-Rad).

Detection of Protease-Inhibition Activity of Aptamers in HeLa Cells—The transfection of cultured cells was as reported previously, with some modifications (*14*). One day before the first transfection, a 24-well plate was seeded with 0.8×10^5 cells per well in D-MEM, 5% heat-inactivated FBS and no antibiotics, and then incubated

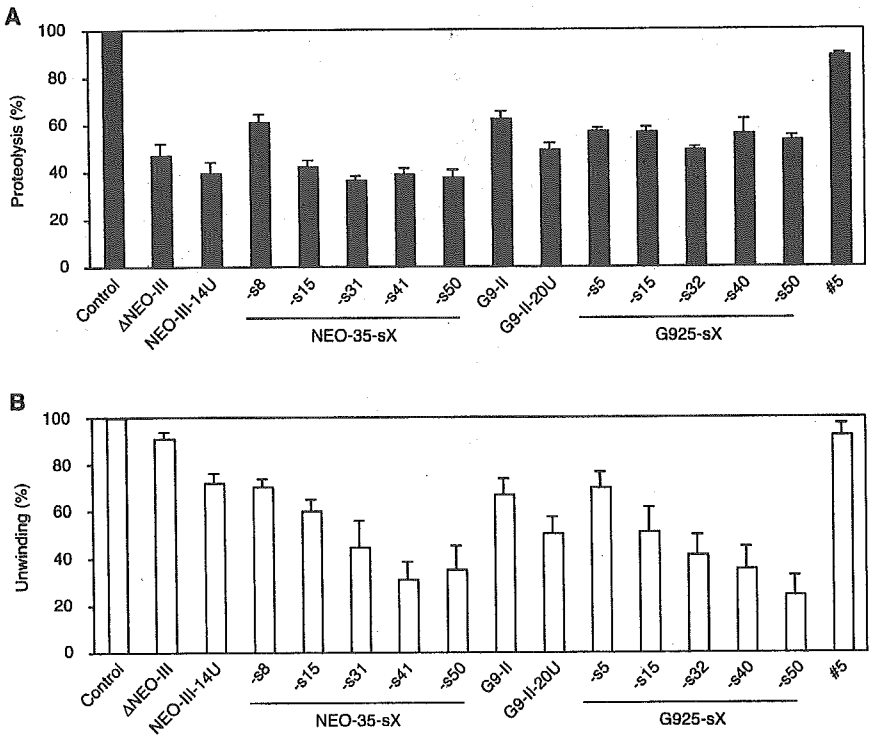

Fig. 2. Screening of ADD aptamers by protease or helicase inhibition assays. (A) Assay for NS3 protease inhibition. The protease-cleavage activity of 1.2 μM NS3 was evaluated in the presence of 1.2 μM aptamers. (B) Assay for NS3 helicase inhibition. The unwinding efficiency of 100 nM NS3 was evaluated in the presence of 25 nM aptamers. The control (100%) in (A) or (B) was the proteolytic or unwinding activity in the absence of RNA.

at 37°C in 5% CO_2. The cells were 70% confluent at the time of transfection. The cells were cotransfected with the NS3-expression vector pCMV/34s-2-FLAG or its mutants pCMV/34s-2-M (500 ng) and the substrate-expression vector pC5abY (25 ng) using Lipofectamine 2000 (1.5 μl; Invitrogen) according to the manufacturer's instructions. pCMV/34s-2-M was used as a negative control. After incubation for 24 h, the cells were transfected with RNA aptamers (90 pmol) using DMRIE-C (4 μl; Invitrogen). Positive and negative control cells were transfected using DMRIE-C without RNA. The cells were incubated for 1 day and harvested in passive lysis buffer (Promega). The fluorescence resonance-energy transfer (FRET) per microgram of total protein in each lysate was measured using a CytoFluor II (excitation at 430 nm; emission at 530 nm; Applied Biosystems). The relative inhibition efficiencies in HeLa cells were calculated from the FRET values using the following equation: inhibition (%) = 100 × [M – R]/[M – W]. M, R and W represent the FRET values of the negative control (NS3 mutant cell lysate), RNA aptamer-transfected cell lysate and positive control (NS3 cell lysate), respectively.

Detection of FLAG Tag Fused NS3 by Immunoblotting—Cell lysates (2 μg total protein) were separated by gradient SDS-PAGE (4–20%; Wako) and transferred to a nitrocellulose membrane (0.1 μm). The membrane was blocked with 10% skimmed milk in Tris-buffered saline with 0.1% Tween 20 (TBS-T). The primary antibody was anti-FLAG M2 monoclonal antibody (Sigma) diluted with TBS-T 10% skimmed milk (1:1,000 dilution). The membrane was washed with TBS-T, and the secondary antibody, HRP-goat anti-mouse IgG HRP (Zymed Laboratories), which was also diluted with TBS-T 10% skimmed milk, was added (1:1,000 dilution). The FLAG-tagged NS3 was detected by enhanced chemiluminescence (Amersham) and by exposure to X-ray film (Kodak).

Preparation of an In Vitro HCV-Replication System—An *in vitro* HCV-replication system was prepared from HCV replicon cells based on the procedure of Hardy *et al.* (*21*). The cells were cultivated in a T-175 bottle until they reached 90% confluence. The cells were harvested, homogenized and the ER membrane fractions (P15) were separated by centrifugation. The P15 fraction was suspended in 100 μl hypotonic buffer [10 mM Tris-HCl (pH 7.8) and 10 mM NaCl] and stored at –80°C. Assays were performed in the presence of RNA aptamers (0.1, 1 and 10 μM), and the products were separated using a 0.8% denaturing agarose gel containing 1× MOPS-EDTA and 18% formaldehyde. The gel was dried and the radioactivity incorporated into the replicated RNA was analyzed using a BAS2500.

RESULTS

Design of Advanced Dual-Functional (ADD) Aptamers—During previous studies of the human HCV NS3, we developed RNA aptamers against the protease and helicase domains: the protease inhibitors were designated G9-I, II and III (*12*), and the helicase inhibitor was designated #5 (*19*). The present study was undertaken to design ADD aptamers against both enzymatic activities of NS3 (Fig. 1). Two different 5′ components were used: ΔNEO-III, which is a minimized form of G9-I (*13*), or G9-II, which is the most efficient aptamer against NS3 protease in HeLa cells (*14*, *15*). Recently, we found that the binding and inhibitory activity of ΔNEO-III for NS3 protein was increased by conjugating an oligo(U) stretch to the 3′-end (NEO-III-14U) (*18*).

Table 1. **IC_{50} against NS3 protease or helicase.**

	Protease (1.2 μM)	Helicase (100 nM)
NEO-III-14U	0.55 ± 0.20 μM	100.0 ± 13.6 nM
NEO-35-s41	0.20 ± 0.02 μM	21.0 ± 7.92 nM
G9-II-20U	0.53 ± 0.17 μM	28.3 ± 7.25 nM
G925-s50	0.26 ± 0.11 μM	17.5 ± 5.59 nM
#5	ND	75.0 ± 35.9 nM

The protease assays were performed in the presence of 0.12, 0.24, 0.6, 1.2, 2.4, 6 and 12 μM aptamer. The helicase assays were performed in the presence of 1–1,000 nM aptamer (NEO-III-14U = 5, 25, 50, 500 and 1,000 nM; G9-II-20U = 1, 5, 10, 25, 50, 100, 500 and 1,000 nM; NEO-35-s41 and G925-s50 = 1, 5, 10, 25, 50 and 100 nM). ND, not detected.

The 3′ component was the #5 helicase aptamer. The 5′ single-stranded region of #5 could be changed to other sequences without structurally changing the 3′-domain (#5Δ) (*19*). The NS3 helicase domain preferentially binds to poly(U) or poly(U/C) tracts in the 3′-UTR of the positive strand [(+) 3′-UTR] of the HCV genome (*17*, *22*). Therefore, we inserted an oligo(U) tract between the 5′ and 3′ aptamers. We expected that the oligo(U) would function as a spacer between the two ADD aptamer domains, thereby preventing steric hindrance and maintaining the aptamer structure on both sides. Two types of ADD aptamer were constructed that simultaneously targeted the two important domains of NS3, NEO-35-sX and G925-sX, which contained spacers of varying lengths (5–50-mers) as indicated by X (Fig. 1).

Selection of the Most Efficient ADD Aptamers—NS3 protease and helicase inhibition assays were used to identify the most efficient inhibitory aptamers among our constructs. Equal amounts of each aptamer were added to a protease-inhibition assay mixture in which NS3 digested a synthetic peptide substrate. The level of inhibition by each anti-protease aptamer was increased slightly by extending an oligo(U) stretch at the 3′-end (Fig. 2A; NEO-III-14U and G9-II-20U). The inhibition efficiencies of the ADD aptamers were similar when either NEO-III-14U or G9-II-20U was used (Fig. 2A). The one exception was NEO-35-s8, with the shortest spacer, which had reduced protease inhibition efficiency. The folding of the NEO-35-s8 secondary structure for both the anti-protease and helicase aptamers was retained even with the U8 spacer. Thus, it appears that steric hindrance associated with the short spacer in NEO-35-s8 prevented it from binding to NS3. NEO-35-sXs showed greater inhibition relative to the G925-sXs aptamers under these conditions, although there seemed to be little difference between them kinetically (as described later).

The partial duplex DNA substrate was unwound by NS3 and the reaction was inhibited in the presence of ADD aptamers. The efficiency of helicase inhibition was increased by extending the length of the spacer (Fig. 2B). This result supports the idea that NS3 predominantly binds to the single-stranded region of ADD aptamers. The unwinding activity of the helicase decreased to 31% with NEO-35-s41 and to 25% with G925-s50. These two conjugated aptamers achieved the greatest inhibition among those tested. We focused next on NEO-35-s41 and G925-s50, and characterized their activity in detail.

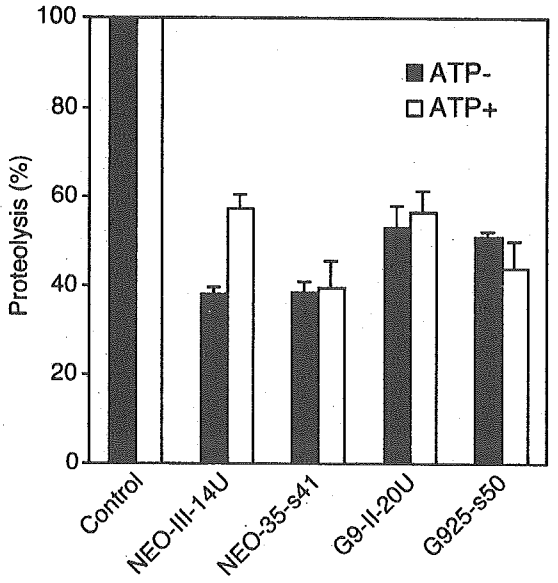

Fig. 3. **Inhibition of NS3 protease activity by aptamers in the presence or absence of ATP.** Equal amounts of each aptamer against 1.2 μM NS3 were added to the NS3 protease assay in the absence or presence of ATP (final concentration = 3 mM), and the reaction mixtures were incubated at 37°C for 20 min.

Determination of IC_{50} against NS3 Protease and Helicase Activities—The kinetics of the NEO-35-s41 and G925-s50 inhibitory activities were analyzed by comparing their NS3 protease and helicase IC_{50} values with NEO-III-14U, G9-II-20U and #5 (Table 1). The IC_{50} of the aptamers against proteolysis was determined using a proteolytic assay containing 1.2 μM NS3 in the presence of 0.12–12 μM of aptamers. The IC_{50} values of NEO-35-s41 and G925-s50 were 0.2 and 0.26 μM, respectively. These values were lower than those for NEO-III-14U (0.55 μM) and G9-II-20U (0.53 μM). The anti-helicase activities were measured using 100 nM NS3 in the presence of 1–1,000 nM aptamers. The IC_{50} values of NEO-35-s41 and G925-s50 were 21 and 17.5 nM, respectively. These values were four-fold lower than that of the anti-helicase aptamer #5 alone (75 nM). Furthermore, G9-II-20U had a lower IC_{50} value than that of the NEO-III-14U. These data imply that ADD aptamers of G9-II types are basically superior to that of NEO-III type in preventing translocation of trapped helicase without #5Δ. Thus it is considered that helicase-inhibitory efficiency is also due to a protease aptamer region of the ADD aptamer in addition to the #5Δ effect.

Inhibition of NS3 Protease Activity in the Presence of ATP—An RNA aptamer with a single-stranded region might become a substrate for NS3 helicase, and might be unwound in the presence of ATP. The protease inhibition activities of the aptamers under helicase working conditions were examined by performing the protease-inhibition assay in the presence of ATP (Fig. 3). NS3 helicase was confirmed to function under the protease-assay conditions (data not shown). Protease inhibition by G9-II-20U, NEO-35-s41 and G925-s50 was unaffected by the presence or absence of ATP. However, the inhibitory abil-

Table 2. **Summary of binding parameters.**

	Low concentration (0.032–4 nM)			High concentration (4–500 nM)		
	B_{max1} (%)	K_{d1} (nM)	n_{H1}	B_{max2} (%)	K_{d2} (nM)	n_{H2}
NEO-35-s41	17.9 ± 1.3	0.19 ± 0.16	1.2 ± 0.4	45.4 ± 1.1	6.99 ± 1.51	1.0 ± 0.1
G925-s50	12.6 ± 0.6	0.11 ± 0.06	1.9 ± 0.3	44.9 ± 1.9	12.0 ± 4.49	1.0 ± 0.2

The parameters were calculated using the non-linear least-squares curve-fitting method (±SD).

ity of NEO-III-14U decreased from 60 to 40% in the presence of ATP. This result is also reflected in the IC_{50} value of helicase (Table 1). It appears that NEO-III-14U is opened and unwound by NS3 helicase in the presence of ATP.

Determination of the Equilibrium-Dissociation Constant and Hill Coefficient—The two ADD aptamers, NEO-35-s41 and G925-s50, showed the strongest helicase-inhibition activity among the constructs tested. The reason for this was investigated by analyzing the binding of NEO-35-s41 and G925-s50 to NS3 at different concentrations under the helicase-assay conditions without ATP. As a result, we observed two plateaus in the binding curves. The first appeared at 1–4 nM of NS3 and ~10–20% of ADD aptamers bound to NS3 (Fig. 4A). The second plateau appeared at over 100 nM NS3, where ~40% of the maximum binding activity was observed (Fig. 4B). The data were fitted by the non-linear least-squares method (see Materials and Methods) under low and high NS3 concentrations (Table 2). This indicated that there are two binding states between ADD aptamers and NS3 that are affected by its concentration: positive cooperativity ($n > 1$) occurs at low concentrations (0.032–4 nM) of NS3 and non-cooperativity ($n = 1$) occurs at high concentrations (4–500 nM) of NS3. This indicates that NS3 can bind more easily to ADD aptamers at low concentrations than at high concentrations.

Electrophoretic Mobility-Shift Analysis (EMSA) by UV Cross-Linking—The complexes formed between ADD aptamers and NS3 were examined directly by performing

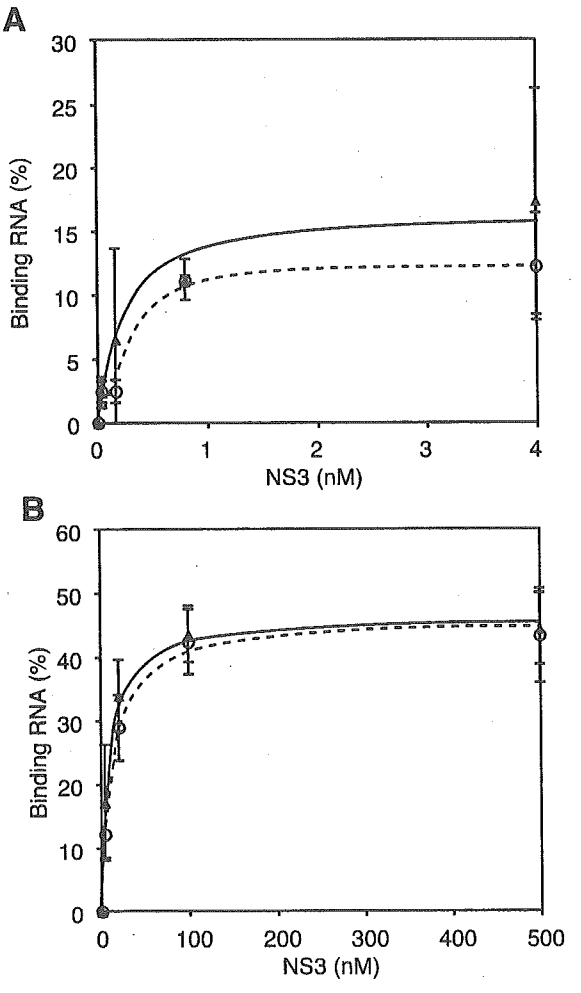

Fig. 4. **Saturated binding curves of NS3 and NEO-35-s41 (filled triangles) or G925-s50 (open circles) were fitted by the non-linear least-squares method.** (A) represents low concentrations of NS3 (0–4 nM), whereas (B) indicates high concentrations (4–500 nM).

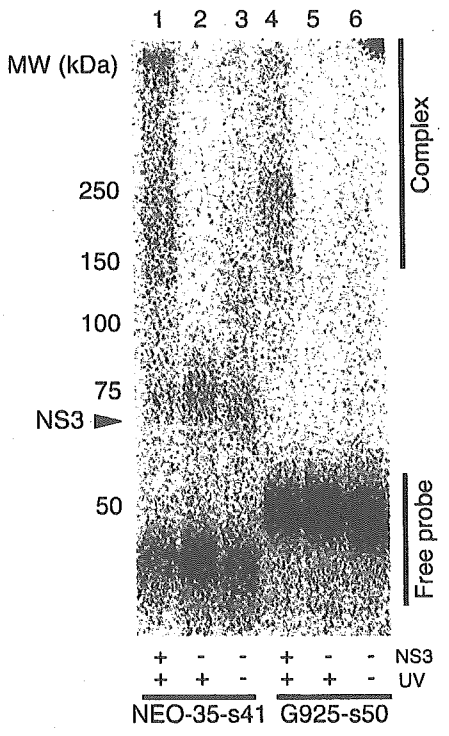

Fig. 5. **EMSA employing UV cross-linking and SDS-PAGE.** The complexes formed between NS3 and conjugated aptamers (internal labeling) were cross-linked by UV irradiation. The samples were then loaded onto a 4–20% gradient SDS polyacrylamide gel. Lanes 1 and 4 were UV irradiated within NS3. Lanes 2 and 5 were UV irradiated without NS3. Lanes 3 and 6 lacked UV exposure and NS3. The molecular sizes of the complexes were estimated by comparison with prestained markers.

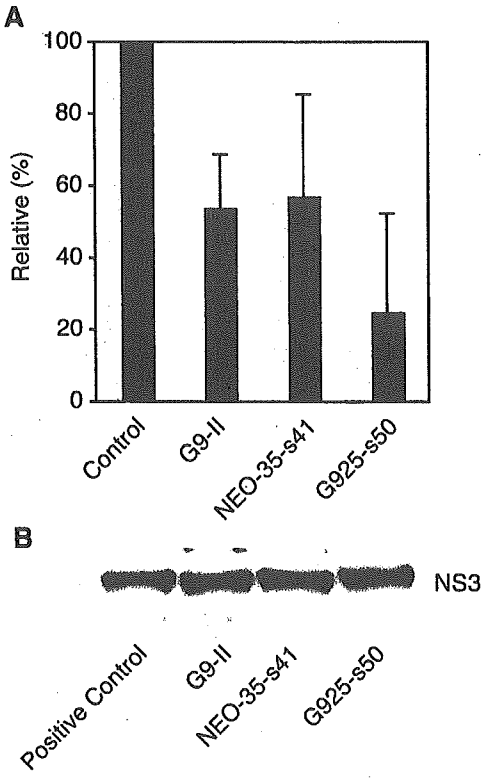

Fig. 6. **(A) NS3 protease-inhibition assay in HeLa cells.** The inhibition efficiency was analyzed by FRET of C5abY substrate protein. **(B) The expression level of FLAG fused NS3 in the cell lysate was assessed by immunoblotting.**

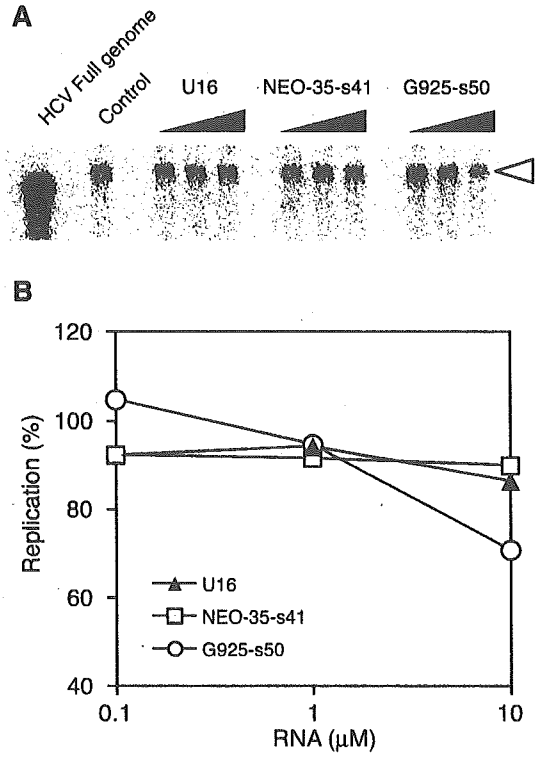

Fig. 7. **HCV genome-replication assay of NEO-35-s41 and G925-s50 using an *in vitro* HCV-replication system.** (A) The reaction mixtures were separated in a 0.8% denaturing agarose gel containing 1× MOPS-EDTA buffer. The open arrowhead indicates the replicated replicon genome. (B) The intensities of the bands from the replicated RNA genome were quantitated using a BAS2500.

EMSA using ^{32}P-labeled aptamers (Fig. 5). The complexes formed by either NEO-35-s41 or G925-s50 with NS3 after UV cross-linking were detected as broad bands with a molecular mass over 150 kDa (lanes 1 and 4). The NEO-35-s41 complex was observed as a band at ~150–250 kDa and also remained within the sample well (lane 1). Interestingly, an 80-kDa band was also observed in the absence of NS3 (lanes 2 and 3), suggesting that NEO-35-s41 forms a dimer. Thus, dimerized NEO-35-s41 must form a macromolecule by binding to several NS3 molecules. In contrast, the size of the complex of G925-s50 and NS3 was ~250 kDa (lane 4). As the molecular masses of G925-s50 and NS3 are ~52 and 70 kDa, respectively, one G925-s50 aptamer could capture three NS3 molecules.

Inhibition of NS3 Protease Activity in HeLa Cell by ADD Aptamers—The inhibitory activity of aptamers within living cells was investigated by transfecting HeLa cells with various different aptamers (90 pmol). The HeLa cells were transiently expressing NS3 and a substrate protein that comprised two types of GFP derivatives connected by a NS3 cleavage site (C5abY) (*14*). This system allows the inhibition of NS3 protease activity to be detected easily by FRET. NEO-35-s41 and G925-s50 caused 45 and 75% inhibition of NS3 proteolysis, respectively (Fig. 6A). NEO-35-s41 achieved the same level of inhibition as G9-II, but G925-s50 was most effective among these three aptamers. The level of NS3 expression was detected by immunoblotting and was not reduced by transfection with aptamers (Fig. 6B). We, therefore, propose that the inhibitory effect of the aptamers is specific for the protease activity of NS3.

Inhibition of HCV Replication Using an In Vitro HCV Replicon Genome-Replication System—We evaluated the ability of NEO-35-s41 and G925-s50 to inhibit HCV replication in an *in vitro* system. The aptamers were added at concentrations of 0.1, 1 and 10 μM (Fig. 7) to a system containing the components of HCV replication, that is, the replicase (non–structural proteins complex) and replicon (genome). The genome can be copied by the replicase in this system (*21*). Thus, this technique is appropriate for the rapid *in vitro* evaluation of the efficiency of HCV-replication inhibitors. The replicated band was detected in the replicon cell lysate but not in the Huh-7 lysate (data not shown). U_{16} (negative control) and NEO-35-s41 did not affect the replication reaction; however, G925-s50 caused moderate inhibition (30%). Our data, therefore, suggest that G925-s50 inhibits the NS3 helicase stage of the replication process.

DISCUSSION

In this study, novel RNA aptamers were designed to attack two important domains of the HCV NS3 protein (ADD aptamer; Fig. 1) simultaneously. As expected, all of

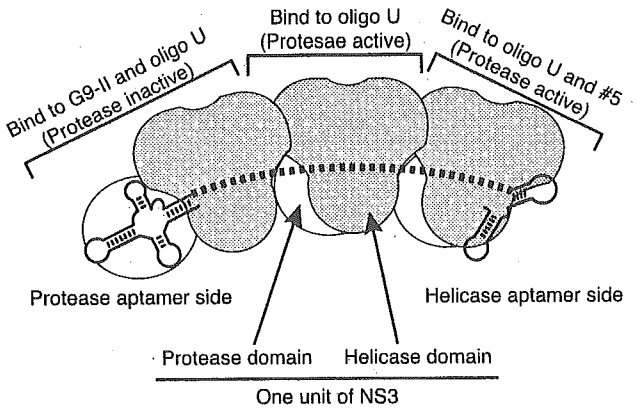

Fig. 8. **Binding model of G925-s50 with NS3. G925-s50 probably binds to three NS3 molecules.** One of the three NS3s binds to the protease aptamer side and inhibits both the protease and helicase activities, while the other two NS3 molecules bind to the central oligo(U) region and the helicase aptamer region to inhibit the helicase activity.

the aptamers had a dual-inhibitory function as a result of conjugating oligo(U) and #5Δ to the NEO-III-14U obtained previously (Fig. 2). Any RNA with a single-stranded region could, in theory, provide a substrate for the NS3 helicase; however, the ADD aptamers did not, and they strongly inhibited both NS3 enzymatic activities (Fig. 3).

Among the constructs tested, NEO-35-s41 and G925-s50 inhibited both the protease and helicase activities of NS3 most effectively. The length of the spacer incorporated into the ADD aptamer affected the efficiency of the inhibition. During HCV replication, the NS3 protein binds to the 3′-UTR, (the site for replication initiation) and unwinds the replicated double-stranded RNA in the 3′ to 5′ direction (*17*). The length of the poly(U/C) tract in the (+) 3′-UTR is important for optimal interaction with NS3; at least 50–62 nucleotides are required for effective replication (*23*). Therefore, we propose that an oligo(U) spacer of 41–50 residues provides an optimal interaction with NS3, enhancing the efficiency of the inhibition by both the anti-protease and anti-helicase aptamers. Furthermore, we reported previously that a variable region in the (+) 3′-UTR regulates the translocation of NS3 helicase, and that the higher-order structure correlates with this regulation (*19*). Accordingly, the slight difference in the efficiency of helicase inhibition by NEO-35-s41 and G925-s50 might be due to the stability of the anti-protease aptamer structure.

The binding of the ADD aptamers NEO-35-s41 and G925-s50 to NS3 was analyzed using a filter-binding assay and EMSA. It appeared that several NS3 molecules efficiently bound to each ADD aptamer. Interestingly, this binding cooperativity varied according to the concentration of NS3: we detected positive cooperativity at low NS3 concentrations and non-cooperativity at high concentrations (Fig. 4 and Table 2). Monomeric NS3 forms dimers or tetramers depending on its concentration (*24*, *25*). The observed change in cooperativity is likely to correspond to the point at which oligomer-formation occurs. Furthermore, EMSA reveals the molecular size of the complex directly (Fig. 5). We could not identify the ratio of NEO-35-s41 to NS3 within this complex, because the NEO-35-s41 dimerized and could form macromolecules with an oligomeric NS3 protein. However, we could clearly identify a 1:3 molar ratio of molecules in the complex between G925-s50 and NS3 (Fig. 8). It is likely that ADD aptamers bind not only to NS3 monomers and dimers, but also to NS3 tetramers. However, as the EMSA was performed under denaturing conditions, only NS3 that was strongly bound to the ADD aptamer would be detected. These data indicate that both NEO-35-s41 and G925-s50 interact strongly with several NS3 molecules, regardless of oligomer formation, and this inhibits helicase and protease activities. Moreover, our results are consistent with the difference observed in inhibition efficiency between protease and helicase activities. We propose that protease inhibition requires a 1:1 stoichiometry between the ADD anti-protease aptamer and NS3, whereas helicase inhibition occurs when several NS3 molecules interact in the region of the oligo(U) spacer and anti-helicase aptamer. G925-s50 appears to trap at least three NS3 molecules and strongly inhibits the sliding of NS3 helicase (Fig. 8).

Two ADD aptamers, NEO-35-s41 and G925-s50, were evaluated as HCV NS3 inhibitors under similar conditions to those found *in vivo* using a protease assay in living cells and an HCV *in vitro* genome-replication system (Figs. 6 and 7). The results of both assays indicated that the aptamer G925-s50 is a more effective inhibitor than NEO35-s41. The efficiency of the two aptamers was similar in the protease inhibition assay. When the inhibitors are applied to living cells, the instability of the NEO-35-s41 structure might be magnified, because the ΔNEO-III aptamer requires more calcium ions than magnesium for the optimal inhibition of NS3 protease, despite the fact that G9-II does not (*13*). Generally, the concentrations of calcium ions are lower than those of magnesium ions in living cells. Furthermore, calcium ions were not added to the *in vitro* HCV genome-replication system, as this might inhibit the effectiveness of NEO-35-s41. Therefore, we suggest that G925-s50 offers advantages in terms of both NS3 protease and helicase inhibition, and should be the candidate of choice for use as an anti-HCV drug. We rationally designed novel ADD RNA aptamers by conjugating two aptamers and adjusting their distance. Additional research on the conjugation of other aptamers will enlarge the field of aptamer application.

We thank Dr. T. Watanabe and Dr. M. Shuda (Tokyo Metropolitan Institute of Medical Science, Japan) for helpful discussions.

REFERENCES

1. Rosenberg, S. (2001) Recent advances in the molecular biology of hepatitis C virus. *J. Mol. Biol.* **313**, 451–464
2. Choo, Q.L., Richman, K.H., Han, J.H., Berger, K., Lee, C., Dong, C., Gallegos, C., Coit, D., Medina-Selby, A., Barr, P.J., Weiner, A.J., Bradley, D.W., Kuo, G., and Houghton, M. (1991) Genetic organization and diversity of the hepatitis C virus. *Proc. Natl. Acad. Sci. USA* **88**, 2451–2455
3. Major, M.E. and Feinstone S.M. (1997) The molecular virology of hepatitis C. *Hepatology* **25**, 1527–1538

4. Grakoui, A., McCourt, D.W., Wychowski, C., Feinstone, S.M., and Rice, C.M. (1993) Characterization of the hepatitis C virus-encoded serine proteinase: determination of proteinase-dependent polyprotein cleavage sites. *J. Virol.* **67**, 2832–2843
5. Tomei, L., Failla, C., Santolini, E., De Francesco, R., and La Monica, N. (1993) NS3 is a serine protease required for processing of hepatitis C virus polyprotein. *J. Virol.* **67**, 4017–4026
6. Kim, D.W., Gwack, Y., Han, J.H., and Choe, J. (1995) C-terminal domain of the hepatitis C virus NS3 protein contains an RNA helicase activity. *Biochem. Biophys. Res. Commun.* **215**, 160–166
7. Failla, C., Tomei, L., and De Francesco, R. (1994) Both NS3 and NS4A are required for proteolytic processing of hepatitis C virus nonstructural proteins. *J. Virol.* **68**, 3753–3760
8. Behrens, S.E., Tomei, L., and De Francesco, R. (1996) Identification and properties of the RNA-dependent RNA polymerase of hepatitis C virus. *EMBO J.* **15**, 12–22
9. De Francesco, R. and Steinkuhler, C. (2000) Structure and function of the hepatitis C virus NS3-NS4A serine proteinase. *Curr. Top. Microbiol. Immunol.* **242**, 149–169
10. Dymock, B.W. and Jones, P.S., and Wilson, F.X. (2000) Novel approaches to the treatment of hepatitis C virus infection. *Antivir. Chem. Chemother.* **11**, 79–96
11. Bianchi, E. and Pessi, A. (2002) Inhibiting viral proteases: challenges and opportunities. *Biopolymers* **66**, 101–114
12. Fukuda, K., Vishnuvardhan, D., Sekiya, S., Hwang, J., Kakiuchi, N., Taira, K., Shimotohno, K., Kumar, P.K.R., and Nishikawa, S. (2000) Isolation and characterization of RNA aptamers specific for the hepatitis C virus nonstructural protein 3 protease. *Eur. J. Biochem.* **267**, 3685–3694
13. Sekiya, S., Nishikawa, F., Fukuda, K., and Nishikawa, S. (2003) Structure/function analysis of an RNA aptamer for hepatitis C virus NS3 protease. *J. Biochem.* **133**, 351–359
14. Kakiuchi, N., Fukuda, K., Nishikawa, F., Nishikawa, S., and Shimotohno, K. (2003) Inhibition of hepatitis C virus serine protease in living cells by RNA aptamers detected using fluorescent protein substrates. *Comb. Chem. High Throughput Screen.* **6**, 155–160
15. Nishikawa, F., Kakiuchi, N., Funaji, K., Fukuda, K., Sekiya, S., and Nishikawa, S. (2003) Inhibition of HCV NS3 protease by RNA aptamers in cells. *Nucleic Acids Res.* **31**, 1935–1943
16. Kanai, A., Tanabe, K., and Kohara, M. (1995) Poly(U) binding activity of hepatitis C virus NS3 protein, a putative RNA helicase. *FEBS Lett.* **376**, 221–224
17. Banerjee, R. and Dasgupta, A. (2001) Specific interaction of hepatitis C virus protease/helicase NS3 with the 3′-terminal sequences of viral positive- and negative-strand RNA. *J. Virol.* **75**, 1708–1721
18. Fukuda, K., Umehara, T., Sekiya, S., Kikuchi, K., Hasegawa, T., and Nishikawa, S. (2004) An RNA ligand inhibits hepatitis C virus NS3 protease and helicase activities. *Biochem. Biophys. Res. Commun.* **325**, 670–675
19. Nishikawa, F., Funaji. K., Fukuda, K., and Nishikawa, S. (2004) *In vitro* selection of RNA aptamer against the HCV NS3 helicase domain. *Oligonucleotides* **14**, 114–129
20. Zuker, M. (1989) Computer prediction of RNA structure. *Methods Enzymol.* **180**, 262–288
21. Hardy, R.W., Marcotrigiano J., Blight, K.J., Majors, J.E., and Rice, C.M. (2003) Hepatitis C virus RNA synthesis in a cell-free system isolated from replicon-containing hepatoma cells. *J. Virol.* **77**, 2029–2037
22. Friebe, P., and Bartenschlager, R. (2002) Genetic analysis of sequences in the 3′ nontranslated region of hepatitis C virus that are important for RNA replication. *J. Virol.* **76**, 5326–5338
23. Yi, M. and Lemon, S.M. (2003) 3′ nontranslated RNA signals required for replication of hepatitis C virus RNA. *J. Virol.* **77**, 3557–3568
24. Levin, M.K. and Patel, S.S. (1999) The helicase from hepatitis C virus is active as an oligomer. *J. Biol. Chem.* **274**, 31839–31846
25. Locatelli, G.A., Spadari, S., and Maga, G. (2002) Hepatitis C virus NS3 ATPase/helicase: an ATP switch regulates the cooperativity among the different substrate binding sites. *Biochemistry* **41**, 10332–10342

Arch Virol (2005) 150: 883–898
DOI 10.1007/s00705-004-0470-0

Archives of Virology
Printed in Austria

Characterization of hypervariable region in hepatitis C virus envelope protein during acute and chronic infection

K. Higashi[1,2], K. Tsukiyama-Kohara[1], T. Tanaka[3], E. Tanaka[4], K. Kiyosawa[4], and M. Kohara[1]

[1]Department of Microbiology and Cell Biology, The Tokyo Metropolitan Institute of Medical Science, Tokyo, Japan
[2]Research and Development Center, International Reagents Co., Sysmex Group, Kobe, Japan
[3]Tokyo Metropolitan Komagome Hospital, Tokyo, Japan
[4]Second Department of Internal Medicine, Shinshu University School of Medicine, Nagano, Japan

Received September 14, 2004; accepted November 19, 2004
Published online January 19, 2005

Summary. Hepatitis C virus (HCV) causes persistent infection in most patients. To clarify the mechanisms underlying establishment of this persistent infection, nucleotide sequences of the E1/E2 region were characterized in 5 patients with acute and chronic HCV infection. We used direct DNA sequencing methods to identify the major sequence of HCV in each patient. Each HCV genome displayed a high frequency of nucleotide sequence variation in the hypervariable region (HVR) of E2. However, patient-specific conserved nucleotide sequences were identified in the E1/E2 region during the course of infection and conserved the higher-order protein structure.

In the acute phase HCV infection, amino acid substitution in HVR-1 as the monthly rate of amino acids substitution per site (%) between each point exceeded 10.2%. In the chronic phase HCV infection, a significantly lower rate of amino acid substitution was observed in patients. The host immune responses to HVR-1 of each HCV isolates from all clinical courses were characterized using synthetic peptides and ELISA. One chronic patient serum (genotype 1b) did not react at all to its own HVR-1 peptides, however another patient (genotype 2b) reacted to all clinical course. These results indicated that HVR-1 might not always exhibit

Note: DDBJ/EMBL/GenBank accession numbers of E1/E2 sequences reported in this paper are AB107929-AB107949.